The 12th Symposium on Polar Science
15 – 18 November 2021

National Institute of Polar Research
Research Organization of Information and Systems

Session IA
Arctic Research

Program and Abstracts

Conveners
Hiroyuki Enomoto, Hiroshi Miyaoka, Kentaro Nishimoto, and Teruo Aoki (NIPR)

【IA】Arctic Research

Scopes

This session invites presentations from a wide range of topics related to the Arctic, including all disciplines of natural sciences, engineering, humanities and social sciences.
The Arctic is experiencing rapid environmental and amplified climatic changes, creating significant challenges for people living in this region and various impacts around the globe. We have been trying to elucidate the whole picture of these changes in the Arctic and their phenomena, but many open questions still remain. The Arctic change also has impacts on the global climate as well as ecosystems and human societies in higher-middle latitudes, which is also a scope of the session.
We welcome the contributions on the latest findings on the ongoing change in the Arctic, as well as its past change and perspectives on future change, improved understanding of processes and mechanisms, its impact on our society.

Conveners : **Hiroyuki Enomoto, Hiroshi Miyaoka, Kentaro Nishimoto, and Teruo Aoki (NIPR)**

Real-time Oral presentations (09:30 – 12:30, 17:00 - 17:45)

Date: Tue. 16 November

	9:20 - 9:30	Opening address by the director-general of NIPR	Takuji Nakamura (NIPR)	
Part 1: Arctic Ocean session Chair: Hiroyuki Enomoto (NIPR)				
IAo1	9:30 - 9:50	Interannual variability of sea-ice age distribution in the Arctic (Invited)	*Noriaki Kimura (Atmosphere and Ocean Reseaerch Institute, The University of Tokyo), Hiroyasu Hasumi (Atmosphere and Ocean Reseaerch Institute, The University of Tokyo), Motomu Oyama(Arctic Sea Ice Information Center, National Institute of Polar Research), Hajime Yamaguchi(Arctic Sea Ice Information Center, National Institute of Polar Research)	IAo1_Kimura_00532_01.pdf
IAo2	9:50 - 10:05	Interannual variability in heat transport of the Pacific Summer Water from Barrow Canyon to the Chukchi Borderland	*Miaki Muramatsu (Hokkaido University / Japan Agency for Marine-Earth Science and Technology), Hiromichi Ueno (Hokkaido University), Eiji Watanabe (Japan Agency for Marine-Earth Science and Technology), Motoyo Itoh (Japan Agency for Marine-Earth Science and Technology), Jonaotaro Onodera (Japan Agency for Marine-Earth Science and Technology), Kohei Mizobata (Tokyo University of Marine Science and Technology)	IAo2_Muramatsu_00337_01.pdf
IAo3	10:05 - 10:20	Ocean wave observation in the Arctic Ocean north of the Laptev Sea	*Takehiko Nose (GSFS The University of Tokyo), Jean Rabault (The Norwegian Meteorological Institute), Takuji Waseda (GSFS The University of Tokyo), Tsubasa Kodaira (GSFS The University of Tokyo), Tomotaka Katsuno (GSFS The University of Tokyo), Naoya Kanna (AORI The University of Tokyo), Kazutaka Tateyama (Kitami Institute of Technology), Joey Voermans (The University of Melbourne)	IAo3_Nose_00617_01.pdf
IAo4	10:20 - 10:35	Roles and effects of inertial sea-ice drift on momentum/heat/salt exchanges at ice*ocean boundary in high-latitude Arctic Ocean: Results from the MOSAiC expedition	*Yusuke Kawaguchi (AORI, U. Tokyo)	IAo4_Kawaguchi_00254_02.pdf
IAo5	10:35 - 10:50	Summary and Highlights of the R/V Mirai Arctic Ocean cruise in 2020	*Shigeto Nishino (JAMSTEC), Amane Fujiwara (JAMSTEC), Motoyo Itoh (JAMSTEC), Jonaotaro Onodera (JAMSTEC), Akihiko Murata (JAMSTEC), Takashi Kikuchi (JAMSTEC)	IAo5_Nishino_00011_01.pdf
IAo6	10:50 - 11:05	Summary of the R/V Mirai Arctic Ocean cruise in 2021	*Amane Fujiwara (JAMSTEC), Motoyo Itoh (JAMSTEC), Jonaotaro Onodera (JAMSTEC), Mariko Hatta (JAMSTEC), Shigeto Nishino (JAMSTEC), Eiji Watanabe (JAMSTEC), Akihiko Murata (JAMSTEC), Takashi Kikuchi (JAMSTEC)	IAo6_Aoki_00091_03.pdf
Part 2: Arctic Atmosphere, Crysopehre and Land session Chair: Teruo Aoki (NIPR)				
IAo7	11:05 - 11:25	Quantifying contributions of external forcings and internal variability to the early twentieth century Arctic warming in Multimodel analysis (Invited)	*Takuro Aizawa (NIPR), Masayoshi Ishii (Meteorological Research Institute), Naga Oshima (Meteorological Research Institute), Seiji Yukimoto (Meteorological Research Institute), Hiroyasu Hasumi (Atmosphere and Ocean Research Institute)	IAo7_Aizawa_00600_01.pdf

IAo8	11:25 - 11:40	Estimates of mass absorption cross sections of black carbon for filter-based absorption photometers in the Arctic	*Sho Ohata (Nagoya University), Tatsuhiro Mori (The University of Tokyo), Yutaka Kondo (National Institute of Polar Research), Sangeeta Sharma (Environment and Climate Change Canada/Government of Canada), Antti Hyv*rinen (Finnish Meteorological Institute), Elisabeth Andrews (University of Colorado, Boulder), Peter Tunved (Stockholm University), Eija Asmi (Finnish Meteorological Institute), John Backman (Finnish Meteorological Institute), Henri Servomaa (Finnish Meteorological Institute), Daniel Veber (Environment and Climate Change Canada/Government of Canada), Konstantinos Eleftheriadis (National Centre for Scientific Research ''Demokritos''), Stergios Vratolis (National Centre for Scientific Research ''Demokritos''), Radovan Krejci (Stockholm University), Paul Zieger (Stockholm University), Makoto Koike (The University of Tokyo), Yugo Kanaya (Japan Agency for Marine-Earth Science and Technology), Atsushi Yoshida (National Institute of Polar Research), Nobuhiro Moteki (The University of Tokyo), Yongjing Zhao (University of California, Davis), Yutaka Tobo (National Institute of Polar Research), Junji Matsushita (National Institute of Polar Research), Naga Oshima (Meteorological Research Institute)	IAo8_Ohata_00556_01.pdf
IAo9	11:40 - 12:00	Heterogeneous response of snow cover in the Northern Hemisphere to the recent Arctic warming (Invited)	*Masahiro Hori (University of Toyama), Masashi Niwano (Meteorological Research Institute), Rigen Shimada (Japan Aerospace Exploration Agency), Teruo Aoki (National Institute of Polar Research)	IAo9_Hori_00096_02.pdf
IAo10	12:00 - 12:15	Concentrations and sizes of black carbon originated from anthropogenic and biomass burning emissions in Northwest Greenland over the past 350 years	*Kumiko Goto-Azuma (National Institute of Polar Research), Yoshimi Ogawa-Tsukagawa (National Institute of Polar Research), Yutaka Kondo (National Institute of Polar Research), Remi Dallmayr (Alfred Wegner Institute for Polar and Marine Research), Jun Ogata (National Institute of Polar Research), Nobuhiro Moteki (The University of Tokyo), Sho Ohata (Nagoya University), Tatsuhiro Mori (The University of Tokyo), Makoto Koike (The University of Tokyo), Kaori Fukuda (National Institute of Polar Research), Motohiro Hirabayashi (National Institute of Polar Research), Sumito Matoba (Hokkaido University), Yuki Komuro (National Institute of Polar Research), Akane Tsushima (Chiba University), Naoko Nagatsuka (National Institute of Polar Research), Koji Fujita (Nagoya University), Naga Oshima (Meteorological Research Institute), Kyotaro Kitamura (National Institute of Polar Research), Kenji Kawamura (National Institute of Polar Research), Teruo Aoki (National Institute of Polar Research)	IAo10_Goto-azuma_00104_02.pdf
IAo11	12:15 - 12:30	Thermokarst subsidence near the settlement in Mayya and Churapcha, eastern Siberia, revealed by ALOS-2 L-band InSAR	*Takahiro Abe (Graduate School of Bioresources, Mie University), Yoshihiro Iijima (Graduate School of Bioresources, Mie University)	IAo11_Abe_00507_01.pdf
Lunch				
Poster short presentation Chair: Hiroshi Miyaoka and Kentaro Nishimoto (NIPR)				
	17:00 - 17:45	3-minute poster appeal (12 short talks of IAp1 – IAp12)		

Poster presentations (16 November - 18 December)

IAp1	Community composition of diatom assemblages in Chukchi Sea under an autumn bloom	*Wakana Amanda Endo (Faculty/Graduate School of Fisheries Sciences, Hokkaido University), Kohei Matsuno (Faculty/Graduate School of Fisheries Sciences, Hokkaido University)	IAp1_Endo_00528_01.pdf
IAp2	Sea ice Floe size distribution during melt season in the Beaufort Sea of the Arctic Ocean	*Shunya Sano (Graduate School of Frontier Sciences, The University of Tokyo / Japan Agency of Marine-Earth Science and Technology, Yokosuka, Japan), Takashi Kikuchi (Japan Agency of Marine-Earth Science and Technology, Yokosuka, Japan / Graduate School of Frontier Sciences, The University of Tokyo), Noriaki Kimura (Atmosphere and Ocean Research Institute, The University of Tokyo)	IAp2_Sano_00525_01.pdf
IAp3	Observation of sea ice using portable passive microwave radiometers in NABOS 2021 expedition	*Kazutaka Tateyama (Kitami Institute of Technology), Naoya Kanna (The University of Tokyo), Takuji Waseda (The University of Tokyo), Hiroyuki Enomoto (National Institute of Polar Research)	IAp3_Tateyama_00176_01.pdf

IAp4	Dynamic ocean topography in arctic sea by Envisat/RA-2	*Keigo Kageyama (Tokyo University of Marine science and technology)	IAp4_Kageyama_00540_01.pdf
IAp5	Numerical Weather Simulations for the Ice Core Drilling Expedition 2021 at SE-Dome, Southeastern Greenland Ice Sheet	*Akihiro Hashimoto (Meteorological Research Institute, Japan Meteorological Agency), Teruo Aoki (Arctic Environment Research Center, National Institute of Polar Research), Tetsuhide Yamasaki (Avangnaq), Sumito Matoba (Institute of Low Temperature Science, Hokkaido University), Masashi Niwano (Meteorological Research Institute, Japan Meteorological Agency), Tomonori Tanikawa (Meteorological Research Institute, Japan Meteorological Agency), Koji Fujita (Graduate School of Environmental Studies, Nagoya University), Yoshinori Iizuka (Institute of Low Temperature Science, Hokkaido University)	IAp5_Hashimoto_00561_01.pdf
IAp6	Is surface darkening occurring over the Greenland Ice Sheet?	*Teruo Aoki (NIPR), Rigen Shimada (JAXA), Masahiro Hori (University of Toyama), Tomonori Tanikawa (Meteorological Research Institute), Masashi Niwano (Meteorological Research Institute)	IAp6_Aoki_00091_02.pdf
IAp7	Integration test of polar regional climate model and radiative transfer model for development of microwave remote sensing simulator	*Rigen Shimada (JAXA), Masashi Niwano (MRI)	IAp7_Shimada_00181_01.pdf
IAp8	Spatial variations in cryoconite holes and phototrophs across an outlet glacier in southwest Greenland	*Nozomu Takeuchi (Chiba University), Koki Ishiwatari (Chiba Univeristy), Akane Watanabe (Chiba University), Takahiro Segawa (Yamanashi University)	IAp8_Takeuchi_00394_01.pdf
IAp9	River surface temperature and channel width in the Arctic region derived from GCOM-C/SGLI	*Masahiro Hori (University of Toyama)	IAp9_Hori_00096_01.pdf
IAp10	Using deep learning to reveal the distribution of thermokarst	*Kosuke Takaya (Graduate School of Agriculture, Kyoto University), Takeshi Ise (Field Science Education and Research Center, Kyoto University)	IAp10_Takaya_00503_01.pdf
IAp11	Proposal for a new fungus genus isolated from Ellesmere Island, Canadian High Arctic	*Masaharu Tsuji (Graduate School of Agriculture, Kyoto University), Yukiko Tanabe (National Institute of Polar Research), Warwick Vincent (Universit* Laval), Masaki Uchida (National Institute of Polar Research)	IAp11_Tsuji_00548_01.pdf
IAp12	Soil bacterial diversity and function in the Canadian Arctic	*Shu-Kuan Wong (NIPR), Ryo Kaneko (BioInsight Co. Ltd.), Masaki Uchida (NIPR)	IAp12_Wong_00484_01.pdf

Interannual variability of sea-ice age distribution in the Arctic

Noriaki Kimura[1], Hiroyasu Hasumi[1], Motomu Oyama[2], Hajime Yamaguchi[2]
[1]*Atmosphere and Ocean Reseaerch Institute, The University of Tokyo*
[2]*Arctic Sea Ice Information Center, National Institute of Polar Research*

Sea ice is a vital component of the global climate system. We need to monitor the current condition of sea ice and to predict the future change of it. Since 1972, observations using satellite microwave sensors have provided continuous images of sea ice . It improved our knowledge of sea-ice cover and its temporal and spatial variability. Ice age also is the important information of sea ice. This study estimates the ice age by a new way based on the backward tracking of sea ice. We first analyze the ice trajectory traced back to the ice formation. Based on the derived trajectory, we examine the sea ice age and other parameters such as traveling distance or accumulated ice convergence.

Daily sea ice velocity was derived from satellite microwave sensor AMSR-E and AMSR2 data. The calculation of the ice drifting speed was based on a pattern matching method, the maximum cross correlation technique (Kimura et al., 2013). This method determined the spatial offset that maximized the cross-correlation coefficient between two brightness temperature arrays in consecutive images separated by 24 hr. After applying filtering and interpolation processes, we constructed a daily ice-velocity dataset without missing data over the sea-ice area on a 60 × 60 km grid for 2003–2021. Backward trajectory is calculated using the daily ice motion. First, particles are arranged at an interval of 10 km over the ice area on a certain day. Daily displacement of particles released on the day is calculated from the ice velocity on one-day time steps. When the particle reaches open ocean (no-ice) area, we assume it to be ice production. In this study, we tracked the particles up to 6 years.

Generally, multi-year sea ice exists the Greenland-Canadian side of the Arctic. The area expands toward the Atlantic side along the north and west coasts of Greenland via the Transpolar Drift Stream and the East Greenland Current, and toward the North American side, moving across the Beaufort Sea to the East Siberian Sea under the influence of the prevailing clockwise Beaufort Gyre. Additionally, narrow branches extending to the New Siberian Island and Severnaya Zemlya. There is a large interannual variability in the ice age distribution. Widespread old ice in the Beaufort Sea observed in 2016 is almost disappeared in 2017. Since then, the old ice in the Beaufort Sea has been gradually increasing (Fig 1). In 2021, a wide area from off the coast of Alaska to near the East Siberian Sea was covered with ice older than three years. A part of this ice remained unmelted during the ice minimum in September, contributing to the large minimum ice extent of this year.

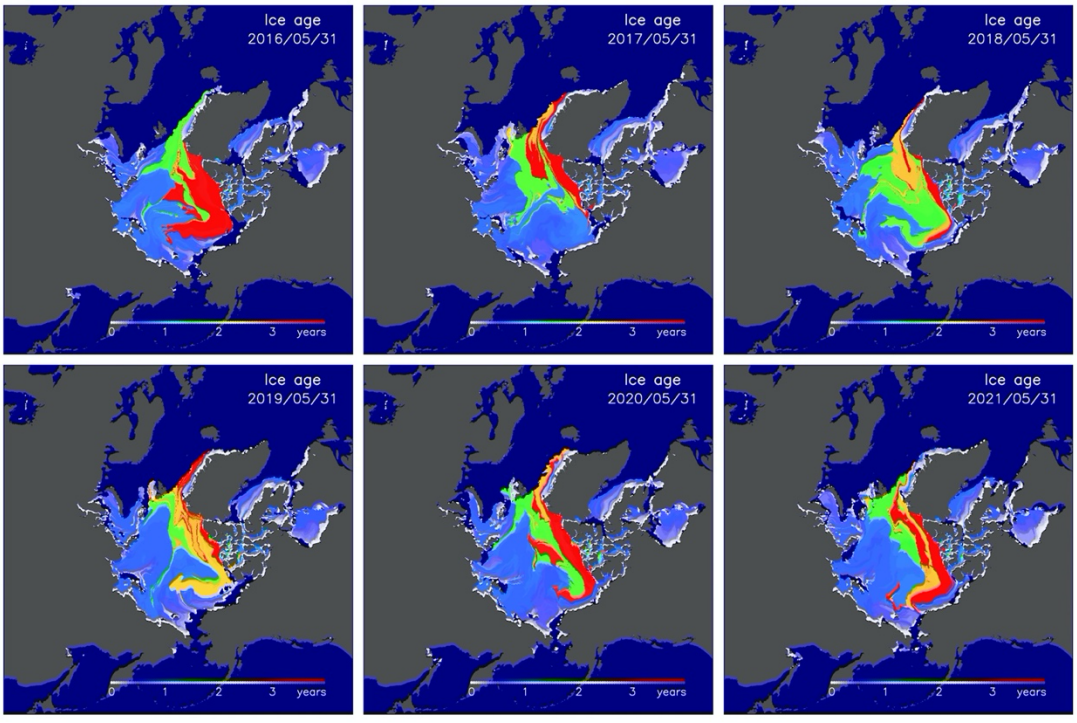

Fig 1.
Ice age distribution of the Arctic Sea ice on May 31 for 2016-2021.

References

Kimura, N., A. Nishimura, Y. Tanaka and H. Yamaguchi, Influence of winter sea ice motion on summer ice cover in the Arctic, Polar Research, 32, 20193, 2013.

Interannual variability in heat transport of the Pacific Summer Water from Barrow Canyon to the Chukchi Borderland

Miaki Muramatsu[1,2], Hiromichi Ueno[1], Eiji Watanabe[2], Motoyo Itoh[2], Jonaotaro Onodera[2] and Kohei Mizobata[3]
[1]*Graduate school/ Faculty of Fisheries Sciences, Hokkaido University*
[2]*Institute of Arctic Climate and Environment Research, Japan Agency for Marine-Earth Science and Technology*
[3]*Department of Ocean Science, Tokyo University of Marine Science and Technology*

The Pacific Summer Water (PSW) enters the Arctic Ocean through the Bering Strait during summer. This PSW inflow could be associated with the sea ice reduction in the Pacific Sector of the Arctic Ocean. The PSW higher than 0°C has the potential to melt sea ice. After passing through the Bering Strait, the PSW reaches Barrow Canyon in the northeastern Chukchi Sea and then turns west. The PSW is transported northwestward along the shelf slope from Barrow Canyon to the Chukchi Borderland by the Chukchi Slope Current (CSC). We investigated the PSW transport and heat loss of the water between Barrow Canyon and St. HSN/NHC on the shelf slope. The mooring data obtained at the stations in Barrow Canyon and St. HSN/NHC indicated that the advection time between Barrow Canyon and St. HSN/NHC was 7–61 days, and that the PSW temperature decreased in the depth of 30–60 m during the transport. This mooring analysis revealed that the subsurface temperature decrease in the 2010s was larger than that in the 2000s. We also investigated interannual variability in the subsurface ocean heat content (OHC) in the Chukchi Borderland using hydrographic data obtained by shipboard survey for 1999–2020, and found that the subsurface OHC showed the positive decadal trend.

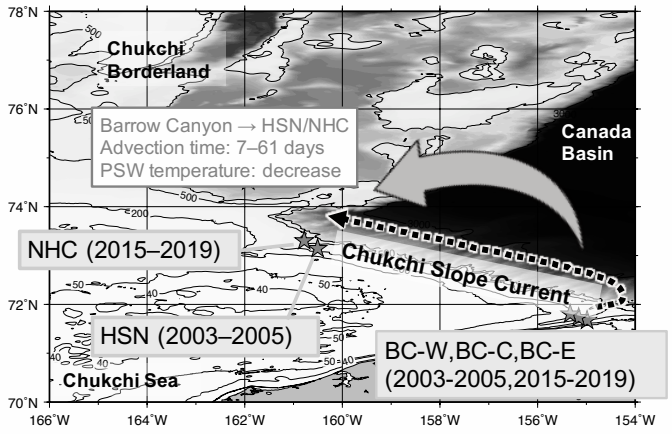

Figure 1. The mooring positions and the Chukchi Slope Current in the northeast Chukchi Sea

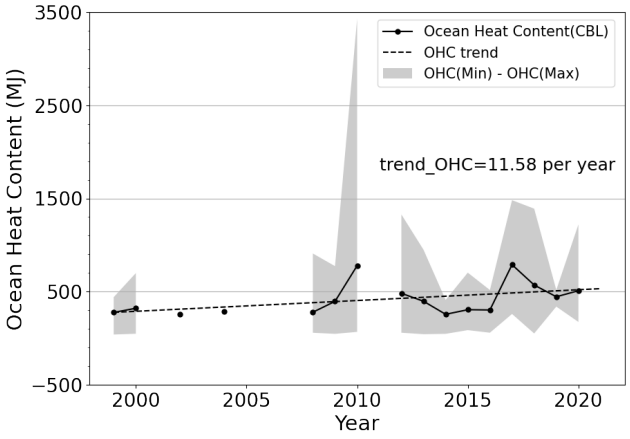

Figure 2. Interannual variability of the subsurface OHC in the Chukchi Borderland.

References

Muramatsu, M., Ueno, H., Watanabe, E., Itoh, M., and Onodera, J., Transport and heat loss of the Pacific Summer Water in the Arctic Chukchi Sea northern slope: Mooring data analysis, Polar Science, in press.

Ocean wave observation in the Arctic Ocean north of the Laptev Sea

Takehiko Nose[1], J. Rabault[2], T. Waseda[1], T. Kodaira[1], T. Katsuno[1], N. Kanna[3], K. Tateyama[4] and J. Voermans[5].
[1]*GSFS, The University of Tokyo,* [2]*The Norwegian Meteorological Institute,* [3]*AORI, The University of Tokyo*
[4]*Kitami Institute of Technology,* [5]*The University of Melbourne*

Extreme waves in the western Arctic Ocean often occurs in the Laptev and East Siberian seas (Waseda et al, 2020), but observations in these waters are scarce. Through the *ArCSII Japan-Russia-Canada International Exchange Program* (https://sites.google.com/edu.k.u-tokyo.ac.jp/arcsii-iep-jrc/main?authuser=0), two drifting wave buoys were deployed in the open water, at 81.92 N 118.75 E north of the Laptev Sea boundary, on 15 Sep, 2021 from *R/V Akademik Tryoshnikov* during the 2021 NABOS expedition (https://uaf-iarc.org/nabos-cruises/). Two types of buoys were deployed: 1). SPOT-1386, which is a SOFAR Spotter buoy (https://www.sofarocean.com/products/spotter), and 2). Zeni-v2021, a revamped version of open source wave-ice buoy (Rabault et al. 2020), using a Zeni Lite drifting buoy as a float for open water application. While both buoys estimate wave statistics from the surface elevation, the difference between the buoys is that SOFAR Spotters measure elevation using the GNSS whereas Zeni-v2021 uses an IMU. SOFAR Spotters battery life is limited at high latitudes due to lack of solar recharge, so SPOT-1386 ran out of battery on 30 Sep.

The buoy tracks and wave statistics, significant wave height H_{m0}, and mean and peak periods T_{m01} and T_p are shown in Figs 1 and 2, respectively. Although the buoys drifted along similar tracks, with the farthest distance of merely 20 km, Fig 2 shows that wave conditions varied considerably between the two buoys. Immediately following the deployment, both buoys measured H_{m0} up to ~1.8 m when the buoys were less than 1 km apart, and the spectra compared well (Fig 3a); however, after this time, even when the buoys distance was < 5 km, H_{m0} varied between the buoys (e.g,. 18 Sep, see Figs 2 and 3b). SPOT-1386 was generally located farther in the marginal ice zone MIZ/ice cover than Zeni-v2021, as such, H_{m0} variation is likely caused by the well-known effect of wave attenuation due to sea ice; this effect warrants quantitative analysis.

Based on the wave spectra and sea ice concentration SIC data, both buoys likely entered ice cover (defined in this abstract as AMSR2 SIC > 0.80) on 27 Sep, 2021. The changes in the Zeni-v2021 spectra are apparent as it entered from open water to an MIZ, then to ice cover, in particular the reduction of noise floor, which has the frequency f^{-4} form (as a result of integrating acceleration twice). With this effect (i.e., the lowered noise floor), it appears that Zeni-v2021 may be capable of estimating small wave heights in ice cover; again, this warrants further analysis. Nevertheless, wave events with H_{m0} up to ~1.0 m have been observed twice by Zeni-v2021 since it entered the ice cover on 27 Sep, and at the time of writing this abstract, it continues to make valuable measurements in the sea with limited observational data.

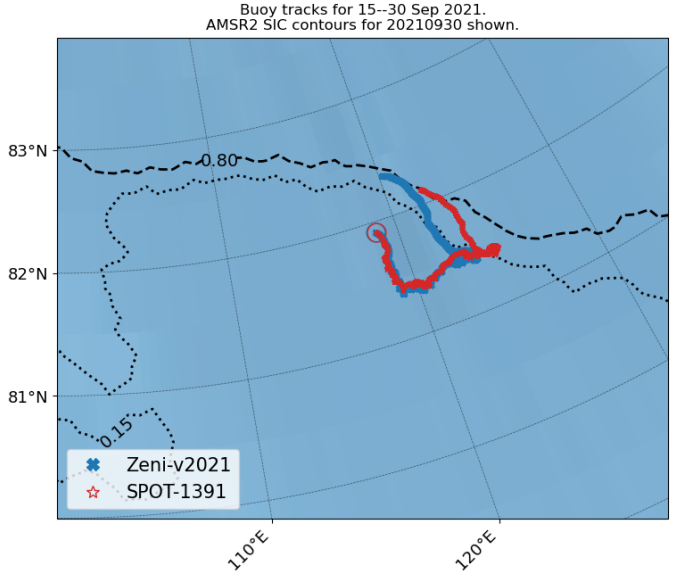

Figure 1. Zeni-v2021 and SPOT-1386 tracks for 15—30 Sep, 2021. AMSR2 SIC contours are shown for 30 Sep. The circle indicates the deployment location.

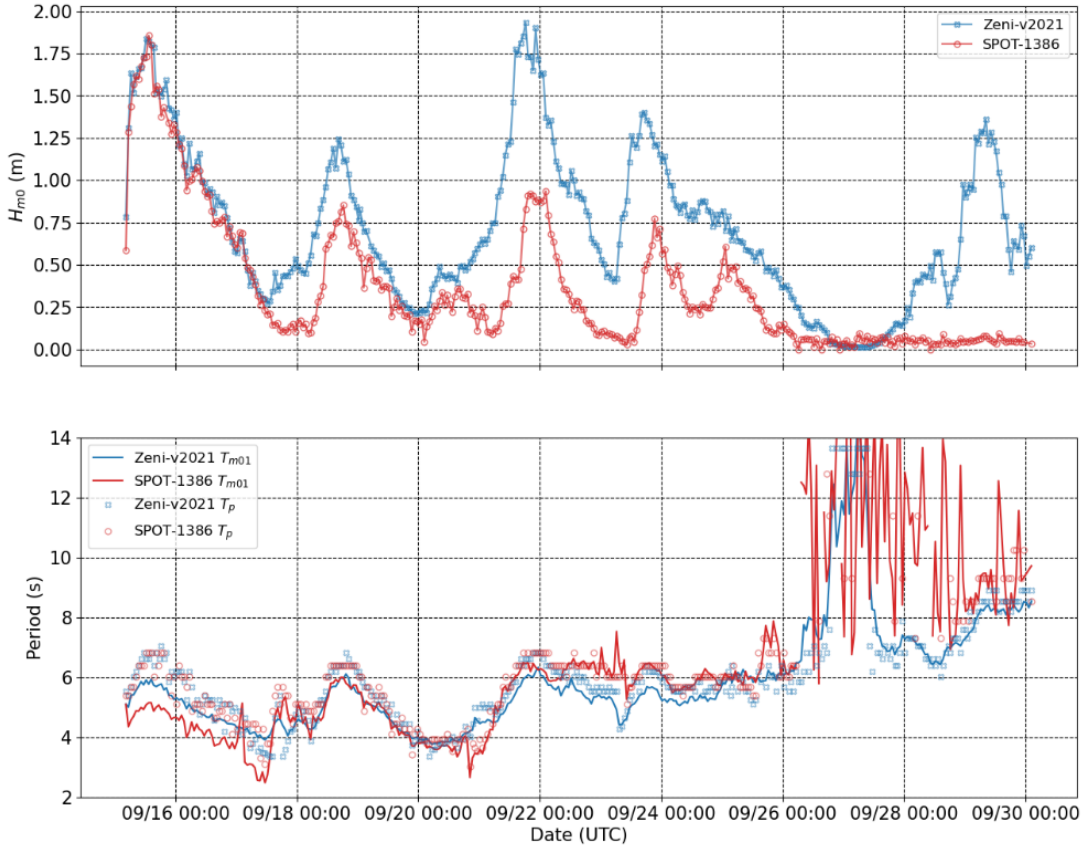

Figure 2. Zeni-v2021 and SPOT-1386 wave height (top) and period (bottom) for 15—30 Sep, 2021. Variation in T_{m01} is partly attributable to integration of different frequency range.

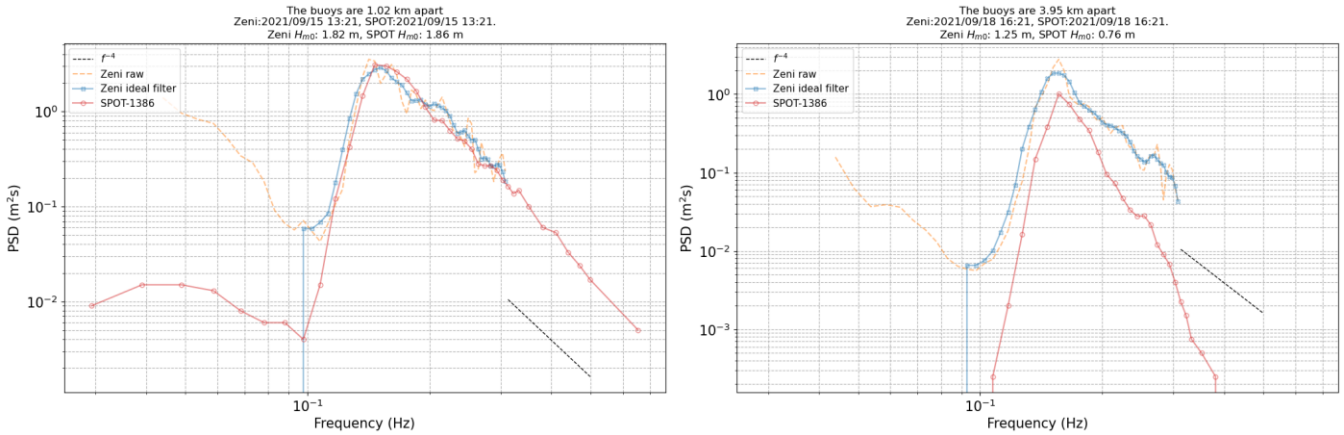

Figure 3. a) Zeni-v2021 and SPOT-1386 surface elevation spectra on 13:21 15 Sep and b) 18:21 21 Sep, 2021. The ideal filter was applied to the smoothed Zeni-v2021 spectra in the same manner as Waseda et al. (2017) to remove the low frequency noise in the open water.

References

Rabault, J. et al. (2020) An open source, versatile, affordable waves in ice instrument for scientific measurements in the Polar Regions, Cold Regions Science and Technology.

Waseda, T. et al. (2017) Arctic wave observation by drifting type wave buoys in 2016, The 27th international ocean and polar engineering conference, international society of offshore and polar engineers. San Francisco, California, USA

Waseda, T. et al. (2020) Climatic trends of extreme wave events caused by Arctic Cyclones in the western Arctic Ocean, Polar Science

Roles and effects of inertial sea-ice drift on momentum/heat/salt exchanges at ice–ocean boundary in high-latitude Arctic Ocean: Results from the MOSAiC expedition

Yusuke Kawaguchi[1], *Zoé Koenig*[2], *Daiki Nomura*[3], *Mario Hoppman*[4], *Jun Inoue*[5], *Ying-Chih Fang*[4], *Kirstin Schulz*[4], *Michael Gallagher*[6], *Christian Katlein*[4], *Marcel Nicolaus*[4], *Benjamin Rabe*[4]

[1] *Atmosphere and Ocean Research Institute, The University of Tokyo, Japan*
[2] *Norwegian Polar Institute, Norway*
[3] *Field Science Center for Northern Biosphere, Hokkaido University, Japan*
[4] *The Alfred Wegener Institute, Helmholz Centre for Polar and Marine Research, Germany*
[5] *National Institute of Polar Research, Japan*
[6] *Physical Sciences Laboratory, National Oceanic and Atmospheric Administration, USA*

This study directly examined the coupling of sea ice and the ocean with emphasis on roles and effects of wind-driven sea-ice drift in the Arctic near the North Pole (Figure a). Observations were conducted for a nearly month from late August through late September, 2020, as the last leg of the international Multidisciplinary drifting Observatory for the Arctic Climate (MOSAiC). The multifarious direct observations of sea-ice and surface water quantified the exchange of momentum, heat, and salt in the ice–ocean boundary layer (IOBL). An array of position buoys (Figure b) was deployed to provide baseline information of geometrical deformation of the ice pack and information elucidating the momentum exchange occurring between sea ice and water for the specific ice floe. Along with the tracked ice motion, sequential profiles of current, hydrography and microstructures were investigated simultaneously. During the observation period, the summertime lowered compactness of pack ice assisted the response of ice drift to surface winds in the absence of internal stress. The swift ice motion caused fully established Ekman currents in IOBL, with vertical scale estimated as 11.7 m (Figure c). The short-term change in ice velocity was characterized mostly by semi-diurnal inertial oscillation, which in turn generated internal waves of similar frequencies in the surface mixed layer. According to rough estimates of turbulent heat and salt fluxes at the ice–ocean interface, an upward shift in freezing temperature resulted from freshened surface water induced a transition from melting to freezing (Figure d). The energetic sea-ice drift amplified the rate of phase change through the turbulent boundary fluxes.

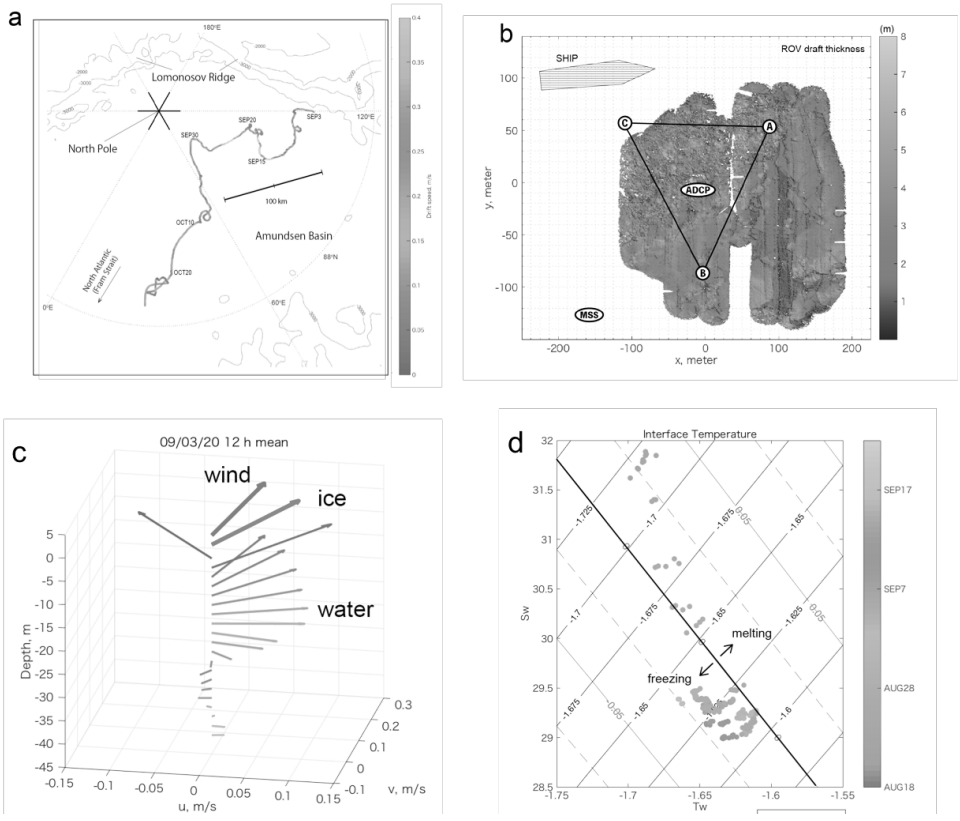

Figure: (a) Trajectory of pack ice of interest, (b) locations of observational instruments installed on the ice floe, where A, B, and C signify GPS ice trackers, ADCP does a current profiler, and MSS does a turbulence device; (c) Ekman spiral observed near the North Pole during the fall leg of MOSAiC expedition; (d) Solutions of interfacial temperature from IOBL heat and salt balance.

Summary and Highlights of the R/V Mirai Arctic Ocean cruise in 2020

Shigeto Nishino[1], Amane Fujiwara[1], Motoyo Itoh[1], Jonaotaro Onodera[1], Akihiko Murata[2],and Takashi Kikuchi[1]
[1]*Institute of Arctic Climate and Environment Research, Japan Agency for Marine-Earth Science and Technology (JAMSTEC)*
[2]*Global Ocean Observation Research Center, Japan Agency for Marine-Earth Science and Technology (JAMSTEC)*

Since spatial and temporal variability is inherently large in the Arctic Ocean, we urgently need baseline data for the Arctic Ocean as a whole to prepare for the further changes to come. Critically needed understandings would be advanced from a coordinated multi-ship, multi-nation pan-Arctic ship-based sampling campaign, based on shared state-of-the-art protocols for data collections and sharing and carefully planned ship tracks during the same period. This could allow for a synoptic view of the totality of hydrographic and ecosystem changes taking place in the Arctic Ocean and facilitate advancing model development using integrated data sets to predict the future state of the Arctic. To obtain such baseline data, we have planned a pan-Arctic research program, the Synoptic Arctic Survey (SAS), with a goal of conducting it in 2020 and 2021.

In 2020, under the SAS program, the Research Vessel (R/V)Mirai conducted hydrographic and biogeochemical surveys, including plankton, microplastic, and bottom sediment samplings, from the Chukchi Sea shelf to marginal ice zones of the Canada Basin (Figure 1). We tried to recover a mooring off Pt. Barrow. Furthermore, a sediment trap was deployed in the Northwind Abyssal Plain, where is on the pathway of the Pacific-origin water, to monitor its transport and impact on marine ecosystem. In a marginal ice zone, we tried to use flying drones to assess the conditions of sea ice and waves. Various drifting buoys were launched to measure the ocean waves, currents, and temperature.

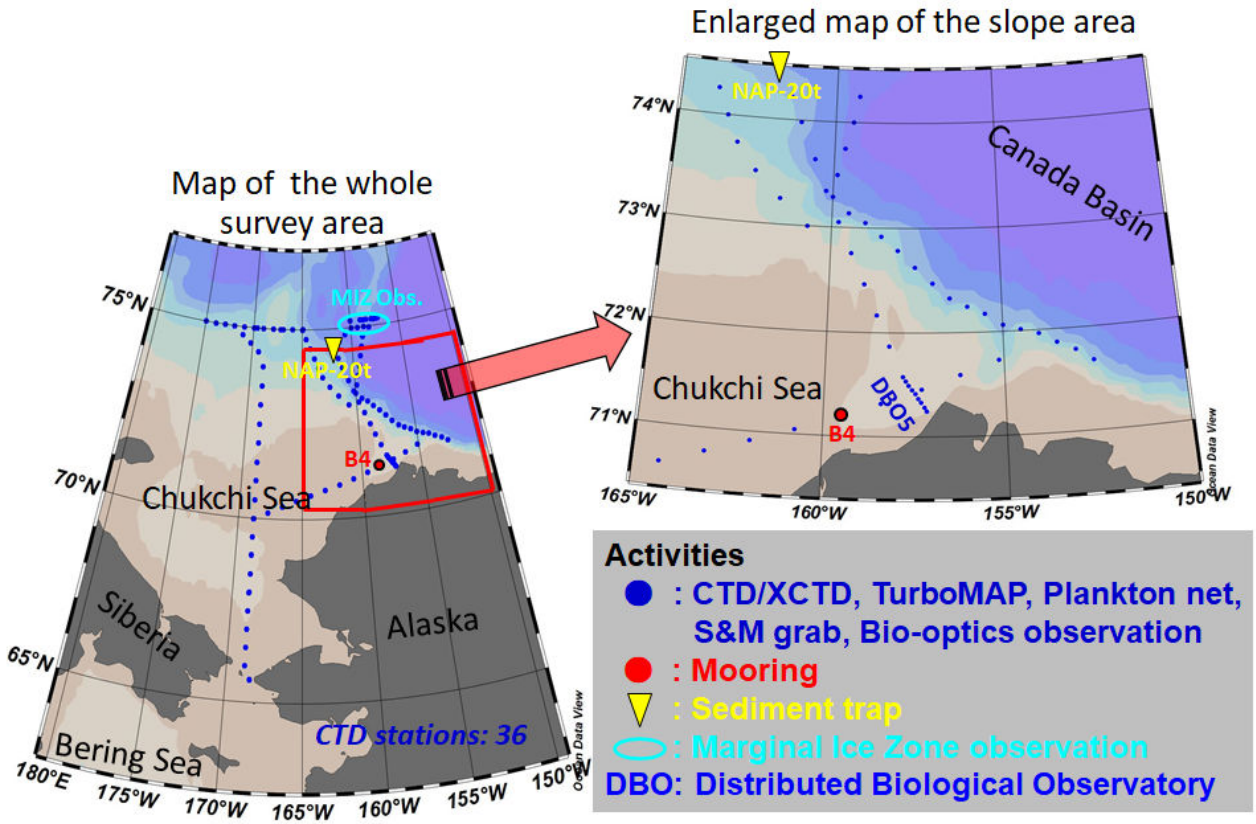

Figure 1. Map of the research areas in the Arctic Ocean (left) and an enlarged drawing from the Chukchi shelf slope to the Canada Basin (right). Blue dots indicate stations where we conducted observations using Conductivity-Temperature-Depth (CTD) sensors with Lowered Acoustic Doppler Current Profiler (LADCP) and water sampling system; eXpendable CTD (XCTD) sensors; Turbulence Ocean Microstructure Acquisition Profiler (TurboMAP); plankton nets; Smith-McIntyre (S&M) grab; and bio-optics instruments. A red dot and yellow triangle represent mooring and sediment trap sites, respectively. A light blue ellipse represents an area of marginal ice zone (MIZ) observation, where we conducted sub-mesoscale observations using XCTD, RINKO-Profiler, and TurboMAP. Various drifting buoys were launched in the MIZ. We also carried out intensive oceanographic surveys off Pt. Barrow under an international collaboration (Distributed Biological Observatory; DBO).

Here we present the following 3 topics.

1) Biological hotspot in the southern Chukchi Sea was not maintained in October 2020. Surface nitrogenous nutrients were not depleted and chlorophyll concentration was lower than usual in autumn.
2) In the marginal ice zone, chlorophyll concentration was relatively high at a seasonal pycnocline (~ 20 m) and below a meltwater front.
3) Aragonite super-corrosive water was found on the Chukchi Plateau (Figure 2), a fishable area (< 2000 m). The corrosive water distribution may be controlled by the extent of Beaufort Gyre. Monitoring of the corrosive water in the Pacific Arctic including the fishable area is necessary under international collaborations of SAS and beyond.

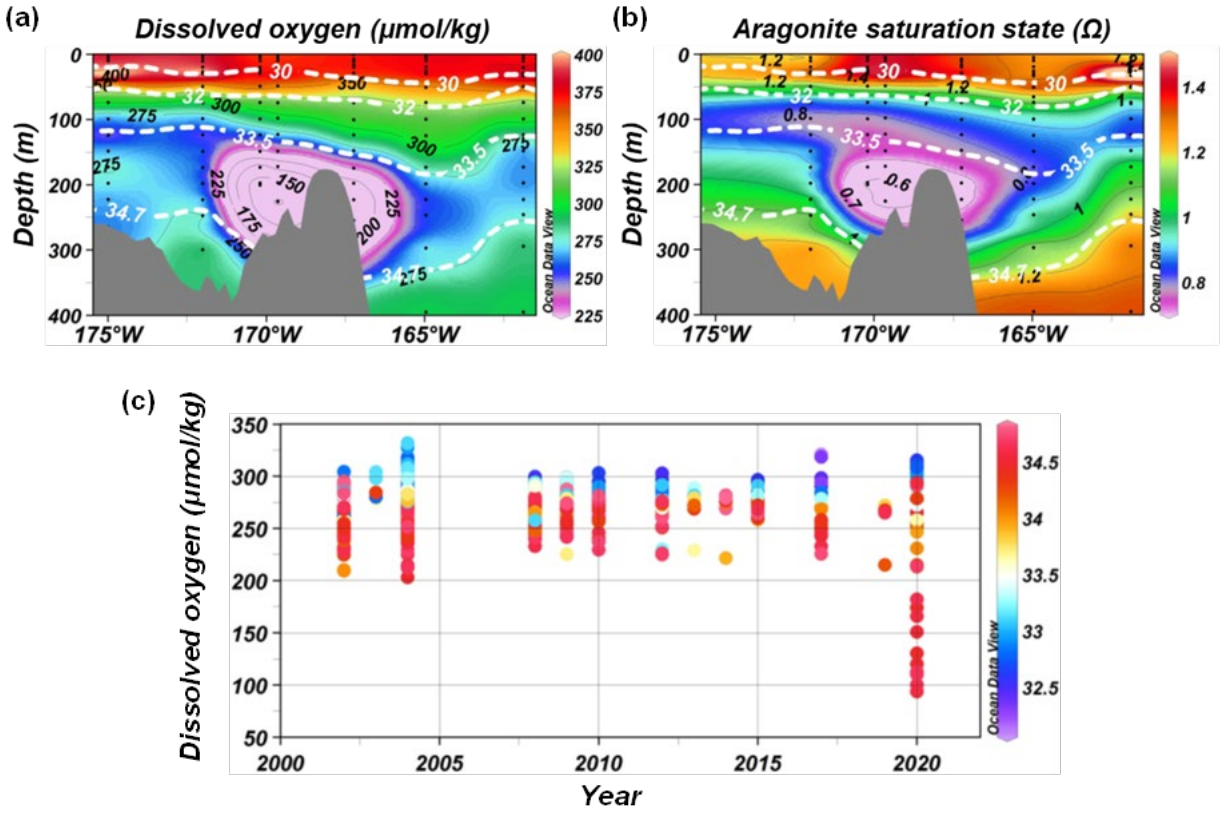

Figure 2. Vertical sections of (a) dissolved oxygen and (b) aragonite saturation state, Ω, along a 75ºN line across the Chukchi Plateau in Figure 1. White dashed-lines indicate salinity. (c) Time series of dissolved oxygen in a water column between 100 and 300 m around the Chukchi Plateau in an area from 172 to 164ºW in longitude and 73.5 to 76.5ºN in latitude. Colors indicate salinity.

Summary of the R/V Mirai Arctic Ocean cruise in 2021

Amane Fujiwara[1], Motoyo Itoh[1], Jonaotaro Onodera[1], Mariko Hatta[1], Shigeto Nishino[1], Eiji Watanabe[1], Akihiko Murata[2], Takashi Kikuchi[1]

[1]*Institute of Arctic Climate and Environment Research, Japan Agency for Marine-Earth Science and Technology (JAMSTEC)*

[2]*Global Ocean Observation Research Center, Japan Agency for Marine-Earth Science and Technology (JAMSTEC)*

The second Arctic observation cruise of the Research Vessel (R/V) Mirai under the framework of Arctic Challenge for Sustainability II (ArCS II) project has been conducted from 31 August to 21 October 2021. The Arctic Ocean has been recognized as a significant area of sea ice reduction, though 2021 was anomalously icy year especially in the Pacific Arctic region (Figure 1). We also found wide-spread less saline water than usual years over the Chukchi Sea shelf region. In this unique year, we collected various hydrographic, atmospheric, and biogeochemical parameters including trace-metals, bacteria, primary productivity, phytoplankton, zooplankton, eDNA, aerosols as well as plastic pollution and surface sediment samples. Three hydrographic moorings and a sediment trap mooring have also recovered and re-deployed on the pathway of the Pacific origin water to monitor its transport and impact on biogeochemical cycles in the region. At the sites near the ice-edge, ice-wave interaction measurements were performed using wave-buoy, radar and flying drone, and sea ice samples were collected for the biogeochemical analyses. The first trials of an in-water drone for the Arctic Ocean were also carried out, which is under developing for autonomously collecting hydrographic and biogeochemical parameters under the sea ice in the future.

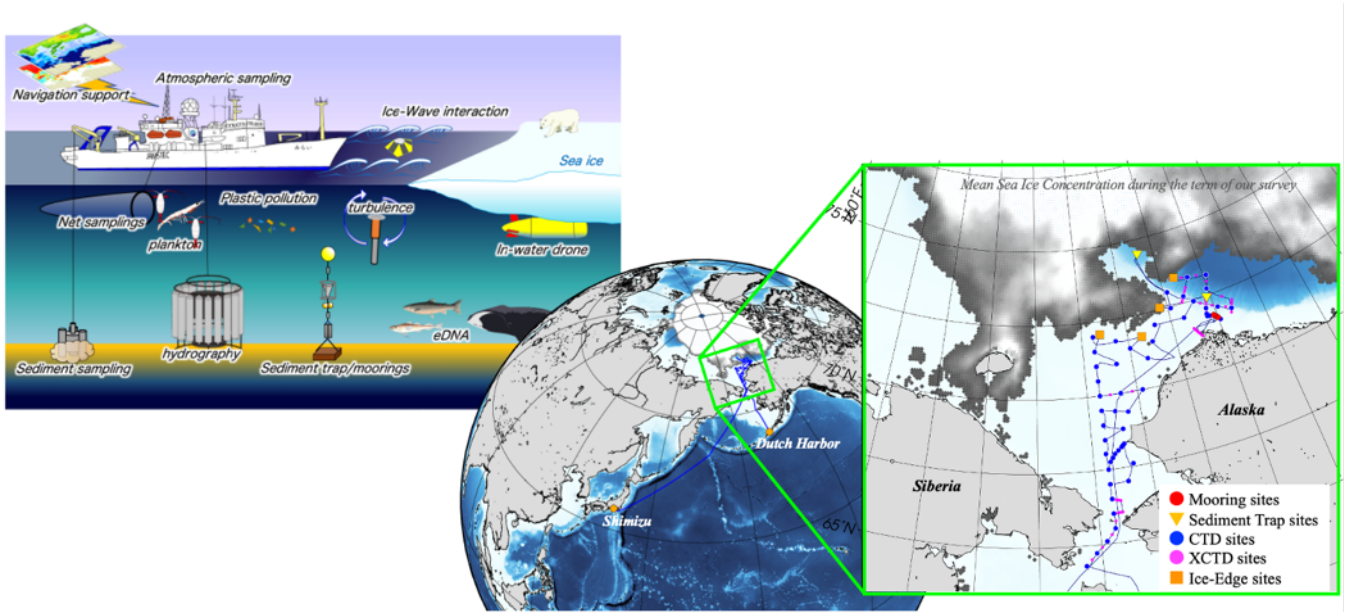

Figure 1. A schematic of the activities conducted during the R/V Mirai cruise of 2021 (left) and the cruise track (right); we departed the port of Shimizu on 31 Aug, entered the Arctic Ocean on 8 Sep, and called the port of Dutch Harbor on 5 Oct.

Quantifying contributions of external forcings and internal variability to the early twentieth century Arctic warming in Multimodel analysis

Takuro Aizawa[1,2], Masayoshi Ishii[2], Naga Oshima[2] , Seiji Yukimoto[2] and Hiroyasu Hasumi[3]
[1]*National Institute of Polar Research*
[2]*Meteorological Research Institute*
[2]*Atmosphere and Ocean Research Institute, The University of Tokyo*

Observational records show significant Arctic warming during the first half of the 20th century comparable to the recent Arctic warming level, which is known as the early 20th century warming (ETCW). It is worth studying to quantify of the contributions of the response to external climate forcing on ETCW using the state-of-the-art climate models of Coupled Model Intercomparison Project Phase 6 (CMIP6). We conducted the multimodel analysis using the Detection and Attribution Model Intercomparison Project (DAMIP) participating climate models to better understand ETCW. The climate simulations in DAMIP mainly consisted of historical simulations (HIST); well-mixed greenhouse-gas-only historical simulations (GHG); anthropogenic-aerosol-only historical simulations (AER); natural solar irradiance forcing and volcanic forcing-only historical simulations (NAT). We also used pre-industrial control simulations (CNTL) of CMIP6 to calculate the contributions of internal variability to ETCW.

Multimodel analysis indicates that, during the ETCW period, the responses of Arctic surface air temperatures (SATs) to increasing greenhouse gases and anthropogenic aerosols were very weak in comparison with the responses of those to the natural forcings. The magnitude of the multimodel mean (MMM) response of Arctic SATs to natural forcings is estimated to be 0.60 ± 0.42°C in the ETCW period, whereas that of the MMM unforced multidecadal internal variability is estimated to be 0.54°C (0.38–0.87°C), suggesting major contributions of the internal dynamics and natural forcings to ETCW.

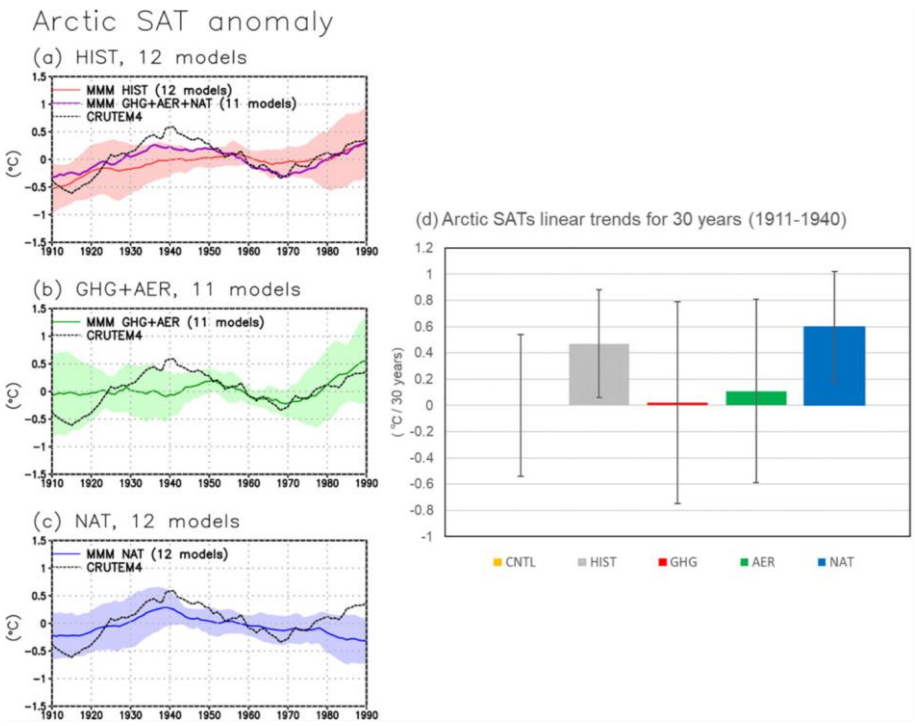

Figure 1. F Time series of the simulated 10-year running mean Arctic SAT anomalies relative to the climatology averaged over latitudes from 60°N to 90°N for (a) HIST and GHG + AER + NAT, (b) GHG + AER, and (c) NAT. The colored lines show the multimodel ensemble means (MMM), including MRI-ESM2.0. The shading indicates the spreads (one standard deviation) based on each member of the 11 or 12 DAMIP models for HIST, GHG + AER, and NAT. The climatology was defined by the mean values from 1941 to 1970. The dashed lines indicate CRUTEM4 observations. (d) The 30-year Arctic SAT linear trends from 1911 to 1940 for HIST, GHG, AER, and NAT. The vertical whiskers in (d) indicate the standard deviation calculated from the 11 or 12 DAMIP models. A leftmost whisker of CNTL in (d) indicates the magnitude (one standard deviation) of the multidecadal internal variability of multimodel. All model-simulated data were interpolated to the CRUTEM4 grid and were masked at grid points missing observations. SAT, surface air temperature; HIST, historical experiments.

Estimates of mass absorption cross sections of black carbon for filter-based absorption photometers in the Arctic

Sho Ohata[1,2,*], Tatsuhiro Mori[3,4,*], Yutaka Kondo[5,*], Sangeeta Sharma[6], Antti Hyvärinen[7], Elisabeth Andrews[8,9], Peter Tunved[10,11], Eija Asmi[7], John Backman[7], Henri Servomaa[7], Daniel Veber[6], Konstantinos Eleftheriadis[12], Stergios Vratolis[12], Radovan Krejci[10,11], Paul Zieger[10,11], Makoto Koike[3], Yugo Kanaya[13,14], Atsushi Yoshida[5], Nobuhiro Moteki[3], Yongjing Zhao[15], Yutaka Tobo[5,16], Junji Matsushita[5], and Naga Oshima[17]

[1]*Institute for Space–Earth Environmental Research, Nagoya University, Nagoya, Aichi, Japan*
[2]*Institute for Advanced Research, Nagoya University, Nagoya, Aichi, Japan*
[3]*Department of Earth and Planetary Science, Graduate School of Science, The University of Tokyo, Tokyo, Japan*
[4]*Department of Physics, Faculty of Science Division I, Tokyo University of Science, Tokyo, Japan*
[5]*National Institute of Polar Research, Tachikawa, Tokyo, Japan*
[6]*Climate Chemistry Measurements Research/Climate Research Division, Environment and Climate Change Canada/Government of Canada*
[7]*Finnish Meteorological Institute, Helsinki, Finland*
[8]*Cooperative Institute for Research in Environmental Sciences (CIRES), University of Colorado, Boulder, CO, USA*
[9]*NOAA Global Monitoring Laboratory, Boulder, CO, USA*
[10]*Department of Environmental Science, Stockholm University, Stockholm, Sweden*
[11]*Bolin Centre for Climate Research, Stockholm University, Stockholm, Sweden*
[12]*Environmental Radioactivity Laboratory (ERL), Institute of Nuclear and Radiological Science & Technology, Energy & Safety, National Centre for Scientific Research ''Demokritos'',Attiki, Greece*
[13]*Research Institute for Global Change (RIGC), Japan Agency for Marine-Earth Science and Technology (JAMSTEC), Yokohama, Kanagawa, Japan*
[14]*Graduate School of Maritime Sciences, Kobe University, Kobe, Japan*
[15]*Air Quality Research Center, University of California, Davis, CA, USA*
[16]*Department of Polar Science, School of Multidisciplinary Sciences, The Graduate University for Advanced Studies, SOKENDAI, Tachikawa, Tokyo, Japan*
[17]*Meteorological Research Institute, Tsukuba, Japan*

Long-term measurements of atmospheric mass concentrations of black carbon (BC) are needed to investigate changes in its emission, transport, and deposition. However, depending on instrumentation, parameters related to BC such as aerosol absorption coefficient (b_{abs}) have been measured instead. Most ground-based measurements of b_{abs} in the Arctic have been made by filter-based absorption photometers, including particle soot absorption photometers (PSAP), continuous light absorption photometers (CLAP), Aethalometers, and multi-angle absorption photometers (MAAP). The measured b_{abs} can be converted to mass concentrations of BC (M_{BC}) by assuming the value of the mass absorption cross section (MAC; $M_{BC} = b_{abs}$/MAC). However, the accuracy of conversion of b_{abs} to M_{BC} has not been adequately assessed. Here, we introduce a systematic method for deriving MAC values from b_{abs} measured by these instruments and independently measured M_{BC}. In this method, M_{BC} was measured with a filter-based absorption photometer with a heated inlet (COSMOS). COSMOS-derived M_{BC} (M_{BC} (COSMOS)) is traceable to a rigorously calibrated single particle soot photometer (SP2) and the absolute accuracy of M_{BC} (COSMOS) has been demonstrated previously to be about 15 % in Asia and the Arctic. The necessary conditions for application of this method are a high correlation of the measured b_{abs} with independently measured M_{BC}, and long-term stability of the regression slope, which is denoted as MAC_{cor} (MAC derived from the correlation). In general, b_{abs}–M_{BC} (COSMOS) correlations were high (r^2 = 0.76–0.95 for hourly data) at Alert in Canada, Ny-Ålesund in Svalbard, Barrow in Alaska, Pallastunturi in Finland, and Fukue in Japan, and stable for up to 10 years. We successfully estimated MAC_{cor} values (10.8–15.1 m^2 g^{-1} at a wavelength of 550 nm for hourly data) for these instruments and these MAC_{cor} values can be used to obtain error-constrained estimates of M_{BC} from b_{abs} measured at these sites even in the past, when COSMOS measurements were not made. Because the absolute values of M_{BC} at these Arctic sites estimated by this method are consistent with each other, they are applicable to the study of spatial and temporal variation of M_{BC} in the Arctic and to evaluation of the performance of numerical model calculations.

Heterogeneous response of snow cover in the Northern Hemisphere to the recent Arctic warming

Masahiro Hori[1], Masashi Niwano[2,4], Rigen Shimada[3,2], Teruo Aoki[4,2]

[1]*University of Toyama*
[2]*Meteorological Research Institute*
[3]*Japan Aerospace Exploration Agency*
[4]*National Institute of Polar Research*

Snow cover is an important geophysical variable to be observed from space for monitoring the effect of the global warming on the Arctic region. We have analyzed the long-term trends of snow cover duration (SCD) in the Northern Hemisphere using satellite-derived snow cover extent products (JASMES/JXAM5, Hori et al., 2017). During the past 37 years (1982-2020, excluding 1994 and 1995 due to poor quality of satellite data), drastic shortening of SCD is seen in the western part of the Eurasia Continent as shown in Figure 1 (a). This shortening has continued through 37 years as also shown in Figure 1(b) and Figure 1(c), which indicate the same maps of SCD trends derived for two different periods (1982-2000, 2001-2020). On the other hand, SCD trends in the North America (NA) continent exhibit spatially and temporally heterogeneous responses. In the former period of 1982-2000 SCD tend to be shorter in the whole NA continent, whereas in the latter period of 2001-2020 SCD trends in mid to eastern part of the NA continent tend to be longer as shown in blue color in Figure 1(c). The lengthening of SCD in NA results both from the delaying of snow melt in spring and earlier snow fall in autumn. Similar lengthening of SCD is also seen in the northern and western part of Scandinavia. These features suggest that the shrinkage and shortening of snow cover in the Northern Hemisphere occurs not uniformly but heterogeneously in space and time.

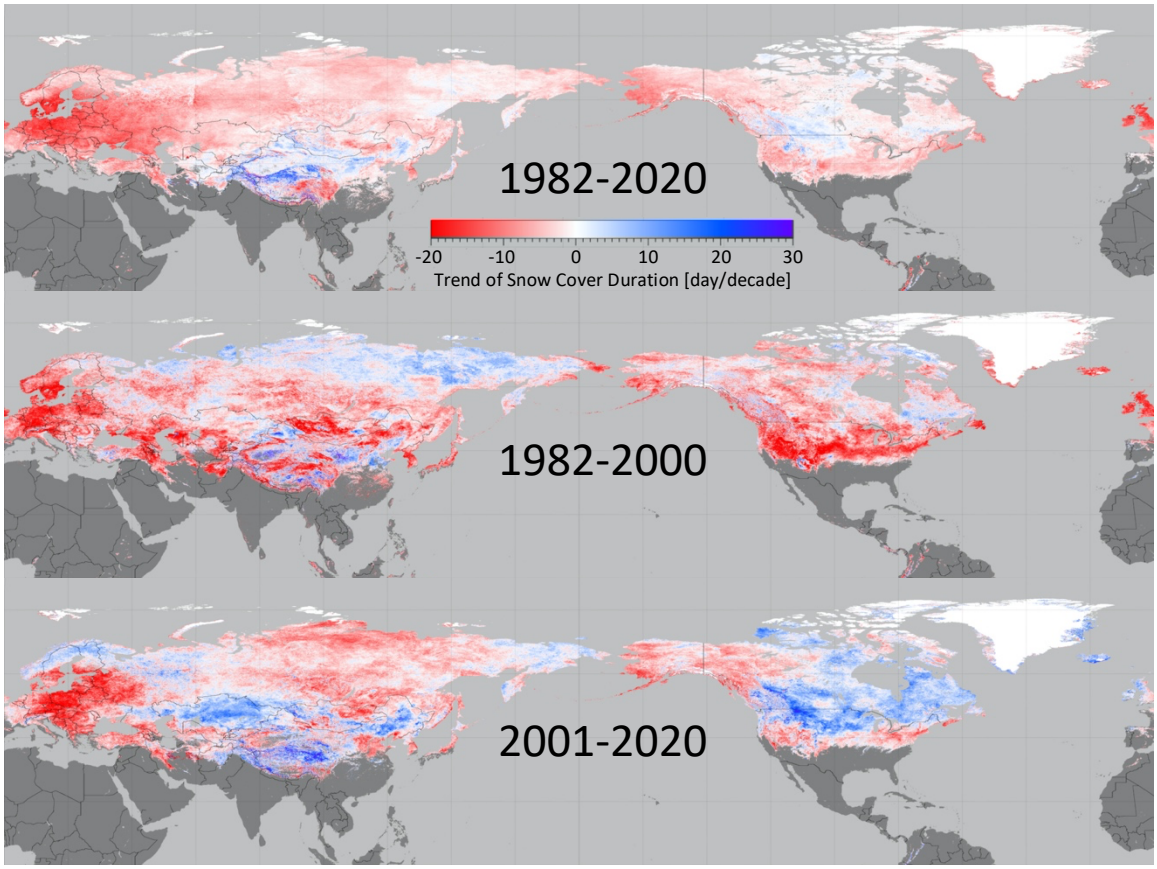

Figure 1. Spatial distributions of long-term trends of snow cover duration (day/decade) in the Northern Hemisphere shown for the period of (a) 1982-2020 (37 years excluding 1994 and 1995), (b) 1982-2000 (17 years excluding 1994 and 1995), and (c) 2001-2020 (20 years).

References

Hori, M., K. Sugiura, K. Kobayashi, T. Aoki, T. Tanikawa, K. Kuchiki, M. Niwano and H. Enomoto, A 38-year (1978–2015) Northern Hemisphere daily snow cover extent product derived using consistent objective criteria from satellite-borne optical sensors, Remote Sensing of Environment, 191, 402-418, https://doi.org/10.1016/j.rse.2017.01.023, 2017.

Concentrations and sizes of black carbon originated from anthropogenic and biomass burning emissions in Northwest Greenland over the past 350 years

Kumiko Goto-Azuma[1, 2], Yoshimi Ogawa-Tsukagawa[1], Yutaka Kondo[1], Remi Dallmayr[1, *], Jun Ogata[1], Nobuhiro Moteki[3]
Sho Ohata[4], Tatsuhiro Mori[3], Makoto Koike[3], Kaori Fukuda[1], Motohiro Hirabayashi[1], Sumito Matoba[5], Yuki Komuro[1]
Akane Tsushima[6], Naoko Nagatsuka[1], Koji Fujita[4], Naga Oshima[7], Kyotaro Kitamura[1], Kenji Kawamura[1, 2], Teruo Aoki[1, 2]

[1]*National Institute of Polar Research, Japan*
[2]*SOKENDAI (The Graduate University for Advanced Studies), Japan*
[3] *The University of Tokyo, Japan*
[4] *Nagoya University, Japan*
[5] *Hokkaido University, Japan*
[6] *Chiba University, Japan*
[7]*Meteorological Research Institute, Japan*
[*] *Present affiliation: Alfred Wegner Institute for Polar and Marine Research, Germany*

Black carbon (BC) is one of the major light-absorbing aerosols, which can affect Earth's radiation budget. BC in the atmosphere absorbs sunlight and heats the atmosphere, whereas BC deposited on snow and/or ice reduces the surface albedo and enhances snowmelt. Black carbon can also act as cloud condensation nuclei and ice nucleating particles, which can play important roles in climate change. To understand the role of BC in climate change, we need long-term data on concentrations and size distributions. The records from the preindustrial period are of special importance in understanding the role of BC in the pristine environment. However, data are still sparse, especially in the Arctic, an important region on Earth where climate and environment have been changing drastically. There have been no direct observations of BC in the preindustrial time, which was unaffected by anthropogenic input. Ice cores can provide proxy records of the past BC concentration and size distribution in the preindustrial period as well as the industrial period.

We analyzed an ice core drilled at SIGMA-D site, Northwest Greenland (Matoba et al., 2015), down to the depth of 113 m using a Continuous Flow Analysis (CFA) system developed at the National Institute of Polar Research. The CFA system enabled us to obtain high-resolution data of BC, stable isotopes of water, microparticles and six elements (Na, K, Mg, Ca, Fe, and Al). For BC analysis, we used a recently developed Wide-range (WR) SP2 (Single Particle Soot Photometer), which can detect BC particles in size range between 70 and 4000 nm (Mori et al., 2016). A combination of WR-SP2 and a high-efficiency nebulizer allowed us accurate measurements of BC concentrations and size distributions. We dated the core by annual layer counting using mainly Na and water stable isotopes. Our ice-core record covers the past 350 years. We divided each year into 12 months and calculated monthly averaged BC concentrations and size distributions.

Both number and mass concentrations started to increase in 1870s due to inflow of anthropogenic BC. The concentrations reached their maxima in 1910s to 1920s, and decreased again since then. The anthropogenic BC shifted the annual concentration peaks from summer to winter-early spring. When anthropogenic BC concentrations decreased to the pre-industrial levels, annual concentration peaks returned to summer again. Anthropogenic BC had larger sizes compared to biomass burning BC. By separating BC in winter and summer using our high temporal-resolution data, we could for the first time reconstruct the temporal variations of BC originated from boreal forest fires including the period with large anthropogenic input. BC originated from boreal forest fires did not show any increasing trend until early 2000s. Our new accurate and high temporal-resolution data on sizes as well as concentrations provide key information to understand sources, transport pathways and deposition processes. Our new data would also contribute to constrain and validate aerosol and climate models. This would lead to better projections of future climate and environment.

References

Matoba, S et al., Glaciological and meteorological observations at the SIGMA-D site, northwestern Greenland Ice Sheet. Bull. Glaciol. Res., 33, 7-10, DOI:10.5331/bgr.33.7 2015.

Mori, T. et al., Improved technique for measuring the size distribution of black carbon particles in liquid water, Aerosol Science & Technology, 50, 3, 242-254, DOI: 10.1080/02786826.2016.1147644, 2016.

Thermokarst subsidence near the settlement in Mayya and Churapcha, eastern Siberia, revealed by ALOS-2 L-band InSAR

Takahiro Abe[1] and Yoshihiro Iijima[1]
[1]*Graduate School of Bioresources, Mie University, Japan*

Thermokarst is an irreversible process with terrain changes induced by ground ice melting in ice-rich permafrost and has been widely observed in eastern Siberia. In the Lena-Aldan interfluve, thermokarst development has been remarkably undergoing in these 30 years (e.g., Fedorov *et al.*, 2014). Thermokarst-induced surface deformation can cause destruction of infrastructure and change in water budget and ecosystems, which impacts the lives of neighbors. In order to predict where and how thermokarst progresses and minimize the impact on local people due to permafrost thaw, it is essential to quantify spatial variation and rate of surface subsidence due to thermokarst development.

Mayya and Churapcha represent the residential areas in the interfluve where thermokarst development has been observed. In Mayya, the averaged thermokarst subsidence rate and its spatial variation in 2015-2018 were revealed by ALOS-2 InSAR stacking (Abe et al., 2020), which corresponds to deforested areas. In Churapcha, Saito *et al.* (2018) used Unmanned Aerial System to derive detailed topographic maps in a disused airfield and arable land and to estimate the surface subsidence since 1990. Iijima *et al.* (in revision) revealed the entire map of thermokarst subsidence in Churapcha between 2015 and 2020 by ALOS-2 InSAR stacking. They revealed activated surface subsidence of 2 cm yr^{-1} in the disturbed area, comprising mainly abandoned agricultural fields. Those studies presented the averaged subsidence rates by the stacking, but did not reveal the temporal changes. Thus, we expanded the analysis period and performed InSAR time-series analysis to derive temporal change of surface displacement.

This study used the GAMMA software to process ALOS-2 L-band SAR data obtained in 2015 and 2020. After co-registration between two SAR images, we created interferograms as much as possible. The topographically-related phase was removed by using ALOS World 3D -30 m- (AW3D30). After excluding some interferograms whose coherence is not good, Small Baseline Subset (SBAS)-type time-series analysis (Berardino *et al.*, 2002; Yanagiya and Furuya, 2020) was performed to derive spatial and temporal changes in surface displacement in Mayya and Churapcha between 2015 and 2020. High-resolution satellite optical images were used to compare the spatial distribution of subsidence with land classification and thermokarst-induced polygonal relief.

The time-series analysis revealed significant surface subsidence up to 6 cm in Mayya and 10 cm in Churapcha between 2015 and 2020. The spatial distributions of subsidence correspond to that of cultivated and post-wildfire sites. Numerous high-centered polygons were identified in the cultivated sites by satellite optical images. It has been considered that ground surface disturbance by cultivation for agriculture/farming and wildfire enhanced thermokarst development compared with non-disturbed areas due to the existence of vegetation.

References

・Abe, T., G. Iwahana, P.V. Efemov, A. R. Desyatkin, T. Kawamura, A. Fedorov, Y. Zhegusov, K. Yanagiya and T. Tadono, Surface displacement revealed by L-band InSAR analysis in Mayya area, Central Yakutia, underlain by continuous permafrost, *Earth, Planets and Space*, 72:138, 2020.

・Berardino, P., G. Fornaro, R. Lanari and E. Sansosti, A new algorithm for surface deformation monitoring based on small baseline differential SAR Interferograms, *IEEE Transactions on Geoscience and Remote Sensing*, 40(11), 2375–2383, 2002.

・Fedorov, A. N., P. P. Gavriliev, P. Y. Konstantinov, T. Hiyama, Y. Iijima and G. Iwahana, Estimating the water balance of a thermokarst lake in the middle of the Lena River basin, eastern Siberia, *Ecohydrology*, 7, 188–196, 2014.

・Iijima, Y., T. Abe, H. Saito, M. Ulrich, A. N. Fedorov, N. I. Basharin, A. N. Gorokhov, V. S. Makaro, Thermokarst landscape development based on multiple spatial data in Churapcha, eastern Siberia, *Frontiers in Earth Science*, in revision.

・Saito, H., Y. Iijima, N. Basharin, A. Fedorov, and V. Kunitsky, Thermokarst Development Detected from High-Definition Topographic Data in Central Yakutia, *Remote Sensing*, 10, 1579, 2018.

・Yanagiya, K. and M. Furuya, Post-wildfire surface deformation near Batagay, Eastern Siberia, detected by L-band and C-band InSAR. *Journal of Geophysical Research: Earth Surface*, 125, e2019JF005473, 2020.

Community composition of diatom assemblages in Chukchi Sea under an autumn bloom

Wakana Amanda Endo[1], Kohei Matsuno[1,2]

[1] Faculty/Graduate School of Fisheries Sciences, Hokkaido University
[2] Arctic Research Center, Hokkaido University

The Arctic Ocean is facing a decrease of sea-ice and an increase of open water period. Chukchi Sea is located in the Pacific sector of Arctic Ocean, which is facing the largest decrease of sea-ice (Selz et al., 2018). Chukchi Sea's high primary production is contributed from phytoplankton, which is mainly composed by diatoms, in water columns and sea-ice algae present under sea-ice. The increase in open water led to an autumn bloom with phytoplankton community change in 2013 (Yokoi et al., 2016, Fujiwara et al., 2018). However, the mechanism of autumn bloom occurrence and diatom species composition in this region is not yet fully understood. The purpose in this study is to clarify the spatial distribution of diatom assemblages in Chukchi Sea during autumn. By comparing with environmental factors, the relationship between environmental conditions and phytoplankton community composition under the bloom.

Surveys by the *R/V Mirai* (Japan Agency for Marine-Earth Science and Technology) were conducted on the 8th, 9th, 26th, and 27th of October 2019 in the range of 163.30.98-169.55.12°W, 64.40.11-71.59.23°N. A CTD cast was made at each station to measure water column temperature, salinity, and density. Water samples were collected from sea surface and from several depths (10, 20, 30, 40m, and chl. *a* max) at each station for nutrient and phytoplankton analysis. 1 L phytoplankton samples were fixed with glutaraldehyde (1% final concentration), and concentrated to 20mL using a syphon, then diatoms were enumerated to species level as much as possible under an inverted microscope.

With 70°N being the border, there was a difference in hydrography and phytoplankton species composition. South to 70°N, nutrients excluding ammonia concentration was low throughout water columns, with no vertical differences in diatom assemblages. North to 70°N, there were distinct stratifications with two types: a thermocline and halocline, with warm surface temperature and low surface saline water. In the northern stations, all nutrient concentrations were low in surface waters, with ammonia and phosphate concentrations being high in the lower layer. Following to the nutrient distribution, diatom cell density was distinctively high in surface layers with a few diatom species. Comparing to the autumn bloom in 2013, it was evident there was an autumn bloom occurring in 2019. This bloom is caused by phytoplankton species favorable in consuming ammonia. As sea-ice decrease in the Pacific sector of Arctic Ocean, light reaching the sea surface will increase and limit nitrification (Shiozaki et al., 2019). Difference in nutrient concentration between these two years caused diatom assemblages to differ from 2013 as well: *Cylindrotheca closterium* and *Leptocylindrus danicus* were dominant species in 2013, whereas in 2019, *Pseudo-nitzschia* spp. dominated in water columns. The dominance by the species could induce negative impact for copepods by stopping their grazing due to domoic acid contained in *Pseudo-nitzschia* spp. (Tammilehto et al., 2012). Such diatom blooms with domoic acid will increase as sea-ice reduces and light-intensity increases in the Pacific sector of Arctic Ocean, indicating primary production may not be transferred as efficiently to higher trophic levels.

References

Selz, V., Laney, S., Arnsten, A. E., Lewis, K. M., Lowry, K. E., Joy-Warren, H. L., Mills, M. M., van Dijken, G. L., Arrigo, K. R., Ice algal communities in the Chukchi and Beaufort Seas in spring and early summer: Composition, distribution, and coupling with phytoplankton assemblages. Limnology and Oceanography, 63, 1109-1133, 2018.

Yokoi, N., Matsuno, K., Ichinomiya, M., Yamaguchi, A., Nishino, S., Onodera, J., Inoue, J., Kikuchi, T., Short-term changes in a microplankton community in the Sea during autumn: consequences of a strong wind event. Biogeosciences, 13, 913-923, 2016.

Fujiwara, A., Nishino, S., Matsuno, K., Onodera, J., Kawaguchi, Y., Hirawake, T., Suzuki, K., Inoue, J., Kikuchi, T., Changes in phytoplankton community structure during wind-induced fall bloom on the central Chukchi shelf. Polar Biology, 41, 1279-1295, 2018.

Shiozaki, T., Ijichi, M., Fujiwara, A., Makabe, A., Nishino, S., Yoshikawa, C., Harada, N., Factors Regulating Nitrification in the Arctic Ocean: Potential Impact of Sea Ice Reduction and Ocean Acidification. Global Biogeochemical Cycles, 10.1029/2018GB006068, 2018.

Tammilehto, A., Nielsen, T. G., Krock, B., Møller, E. F., Lundholm, N., *Calanus* spp.-Vectors for the biotoxin, domoic acid, in the Arctic marine ecosystem?. Harmful Algae, 20, 165-174, 2012.

Sea ice Floe size distribution during melt season in the Beaufort Sea of the Arctic Ocean

Shunya Sano[1,2], Takashi Kikuchi[1,2], and Noriaki Kimura[3]
[1]*Graduate School of Frontier Sciences, The University of Tokyo*
[2]*Japan Agency of Marine-Earth Science and Technology, Yokosuka, Japan*
[3]*Atmosphere and Ocean Research Institute, The University of Tokyo*

Introduction

Sea ice plays an important role in the polar climate system due to its ability to reduce heat transfer from the ocean to the atmosphere and its high reflectivity of solar radiation. Especially in the seasonal ice zone (SIZ), the behavior of sea ice, has a significant impact on not only climate change in the surrounding region but also marine ecosystem and local communities. As the proportion of SIZ is increasing in the Arctic Ocean, it will become increasingly important to understand the dynamical processes of SIZ. To understand the behavior of the SIZ, which is composed of ice floes of various sizes, knowledge of sea ice floe size distribution (FSD) is indispensable.

In the previous studies of FSD, the cumulative number distribution of sea ice, N(d), defined as the number of floats with a diameter less than or equal to d per unit area, has been found to follow the power law, $N(d) \propto d^{-\alpha}$(Eq.(1)) (e.g., Toyota et al., 2006; 2016, Horvat et al., 2019). However, detailed time-evolution of FSD is not yet well-known. The study of changes of FSD in SIZ can contribute to the improvement of the performance of numerical models of the Arctic Ocean, since the effect of different ice floe sizes on melting is very different for the same sea ice concentration. In this study, we focus on changes of FSD during sea ice melt season in the Beaufort Sea of the Arctic Ocean using satellite observation data.

Data and analytical methods

To understand changes of FSD in the Beaufort Sea, we used MODIS (Moderate Resolution Imaging Spectroradiometer) data. Large-scale ice floes in the Beaufort Sea were analyzed from a 500 km × 500 km MODIS Level 1B Channel 1 visible image projected onto a 250 m resolution polar stereographic image. Since MODIS images assume the presence of clouds, we selected images that were almost cloud-free in the observation area and suitable for analysis.

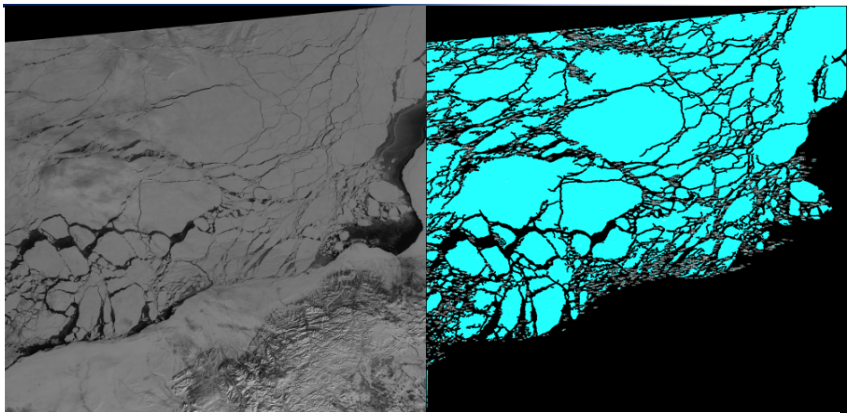

Figure 1. MODIS image (Left) and FSD analysis image (Right) on April 04, 2020.

FSD were calculated from MODIS satellite imagery along the Beaufort Sea (2018 - 2020) and buoy tracks (2018, 2020). Image analysis was performed using the image processing software “ImageJ” (Image processing and Analysis in Java). Figure 1 shows MODIS satellite image and FSD analyzed image by ImageJ on April 04, 2020. The land and fixation surface, which are not subject to analysis, were masked, and the image was binarized to emphasize the edges. The area of the sea ice was converted to the size of the ice floe in pixels. In this study, the ice floe size (d) was evaluated as $d = \sqrt{4A/\pi}$. Then, we counted the sea ice for each ice floe size (FSD). We conducted two types of analysis to find FSD evolution during melt season. First, the Lagrangian analysis along the trajectory of ice-drifting buoy (sea ice tracked) was performed. We used two buoys’ datasets obtained by JAMSTEC ice-drifting buoy deployed in the Beaufort Sea in March 2018 and March 2020 (Kimura et al., 2021). Second, the Eulerian analysis (fixed location analysis) focused on the area off Utqiaġvik (Barrow), Alaska to understand interannual variation of FSD. Based on the previous studies, we studied a relationship between sea ice floe size and the cumulative number distribution of sea ice, N(d), and estimate the value of α which is the exponent number of (1). Note that because of the resolution and width of the MODIS image and this analytical method, we can detect number distribution of sea ice floe size between 300m and 100km.

Results

Figure 2 shows cumulative number distributions of sea ice, N(d), versus sea ice floe size from day 95 (April 4) to day 179 (June 28), 2020, along the track of ice-drifting buoy deployed in March 2020 (The Lagrangian analysis). Then, we calculated

α in Eq.(1) of each line of FSD (Fig.2). The Lagrangian analysis along the buoy trajectory clearly captured that α increased from 1.05 (day 95) to 3.07 (day 179). It means that the number of smaller size ice floes increase and the larger size ice floes decrease (or disapper) as the number of days increases during sea ice melt season. We also carried out the same analysis using the data in 2018. Although the satellite data in June and later when large decreases in sea ice are expected were not available due to the existence of clouds, the number of α slightly increase between March and May.

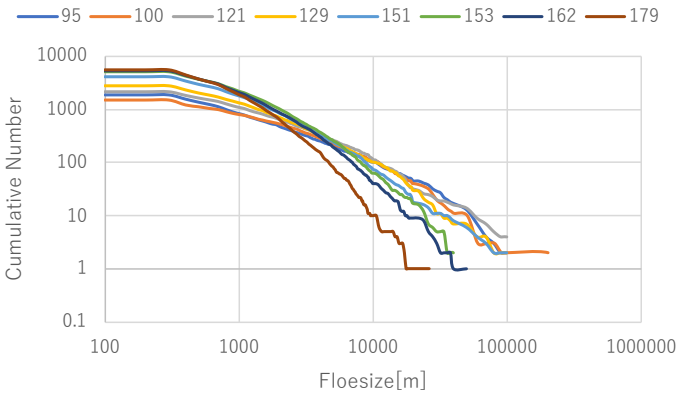

Figure 2. cumulative number distributions of sea ice, N(d), versus sea ice floe size from day 95 (April 4) to day 179 (June 28), 2020, along the buoy track.

We investigate changes of FSD and α of the satellite images obtained in the areaoff Utqiaġvik (Barrow), Alaska (Eulerian analysis) in 2018-2020. For example, the α increased slightly from 1.28 (day 91) to 1.99 (day 157) in 2020. Note that such increases in α can be found in this area all years (2018-2020). We will extend analysis period before 2018 to understand a characteristics of the FSD change during melt season and its interannual variability.

Concluding remarks

In this study, we first established a method for estimates of sea ice floe size distribution (FSD) using MODIS satellite data and image processing software. Then, we investigate changes of FSD during sea ice melt season in the Beaufort Sea of the Arctic Ocean. We found the an increase in α of Eq.(1) in both Lagrangian and Eulerian analysis. In particular, in the Lagrangian analysis along the buoy track in 2020, the value of α increased from 1.05 to 3.07 with the melting of sea ice between March and July 2020. This indicates that the number of large ice floes decreased whereas the number of small ice floes increased. We continue to analyze FSD in the Beaufort Sea during melt season using satellite data before 2018 for more better understanding of change of FSD and sea ice melting process.

Acknowledgments

The MODIS dataset used in this study were acquired from the Level-1 and Atmosphere Archive & Distribution System (LAADS) Distributed Active Archive Center (DAAC) (https://ladsweb.modaps.eosdis.nasa.gov/). The image processing software “ImageJ” (Image processing and Analysis in Java) used in this study was downloaded from the following site (https://imagej.nih.gov/ij/).

References

Horvat1, C., L. A. Roach, R. Tilling, C, M. Bitz, B. Fox-Kemper, C. Guider, K. Hill, A. Ridout, and A. Shepherd, Estimating the sea ice floe size distribution using satellite altimetry: theory, climatology, and model comparison, The Cryosphere, 13, 2869–2885, https://doi.org/10.5194/tc-13-2869-2019, 2019.

Kimura, S., T. Kikuchi, A. Fujiwara, A, Mahoney, H. Eicken, and T. Goda, Sea-ice motion and oceanographic data from the Beaufort Sea to the Chukchi Borderland in March–December 2020, Polar Data Journal, 5, 60-68, 2021.

Toyota, T., S. Takatsuji, and N. Nakayama, Characteristics of seaice floe size distribution in the seasonal ice zone. Geophys. Res. Lett., 33, L02616. http://dx.doi.org/10.1029/2005GL024556, 2006.

Toyota, T. and Alison, K, Alexander D. Fraser, Formation processes of sea ice floe size distribution in the interior pack and its relationship to the marginal ice zone off East Antarctica, Deep-sea Res. II 131, 28-40, 2016.

Observation of sea ice using portable passive microwave radiometers in NABOS 2021 expedition

Kazutaka Tateyama[1], Naoya Kanna[2], Takuji Waseda[3] and Hiroyuki Enomoto[4]
[1]*School of Earth, and Environmental Engineering, Kitami Institute of Technology*
[2]*Atmosphere and Ocean Research Institute, The University of Tokyo*
[3]*Department of Ocean Technology Policy and Environment, Graduate School of Frontier Sciences, The University of Tokyo*
[4]*Arctic Environment Research Center, National Institute of Polar Research*

The NABOS 2021 expedition aboard R/V Akademik Tryoshnikov took place during the period from 10 September to 19 October 2021 in the Russian side of the Arctic Ocean, as shown in Fig. 1. The purpose of this study was to develop an algorithm for estimating sea ice thickness using the satelliteborne passive microwave radiometer AMSR2. We performed onboard and on ice observations using the portable Passive Microwave Radiometer (PMR) as shown in Fig. 2 and Table.1. On the ship, three insturemnets of PMR and an infrared camera wewe used over various ice conditions such as open water, new ice, young ice, and first-year ice. On ice staion, thin first-year ice (40 - 50 cm thick), medium first-year ice (100 cm thick), and deformed ice (140 cm thick) were observed with PMRs as well, and then temperature, salinity, density, and crystal structure of snow and sea ice were measured in the areas coresponding to the field of view of PMR instrument.

Figure 3 shows an example of results of observation on ship. While ship stops for the CTD cast, different types of sea ice were measured by PMRs in the different place and surface conditions ranged from the open water to first-year ice. As a result, the brightness temperature and the difference between the horizontal polarization and the vertical polarization for open water and new ice showed low value and large difference, respectively, whereas the brightness temperatures and the difference between the polarizations increase and decrease, respectively, with ice growth from new ice to first-year ice. The residual first-year ice showed in the rightmost ice type in Fig.3 indicated that higher the frequencies tend to show lower brightness temperature.

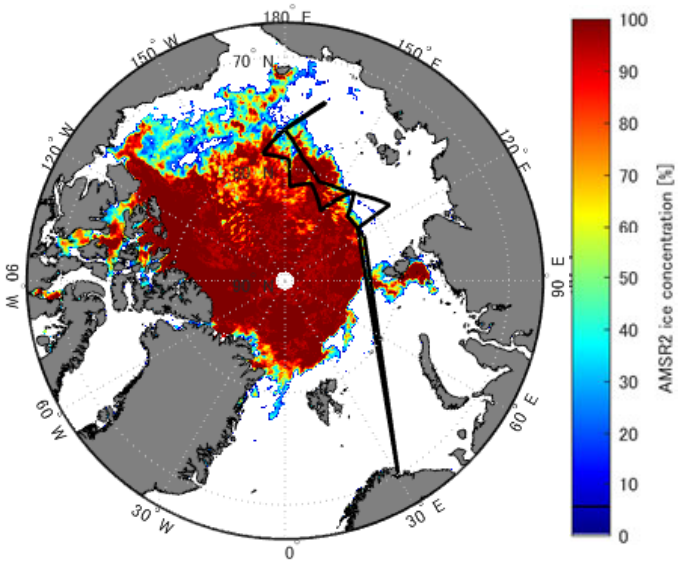

Figure 1 Scheduled observation route of NABOS 2021(black line) and AMSR2 sea ice cconsetration (color) on 6 September 2021.

Table 1 Specifications of the MMRS2C

	MMRS2C-6GHz	MMRS2C-18GHz	MMRS2C-36GHz
Frequency Band	6.925GHz ±0.2GHz	18.7GHz ±0.3GHz	36.5GHz ±0.7GHz
Polarization	Vertical and Horizontal		
Accuracy	1K @300K		
Field of view	15 deg	10 deg	7 deg

Figure 2 Photo of PMR (MMRS2C-36GHz) observation.

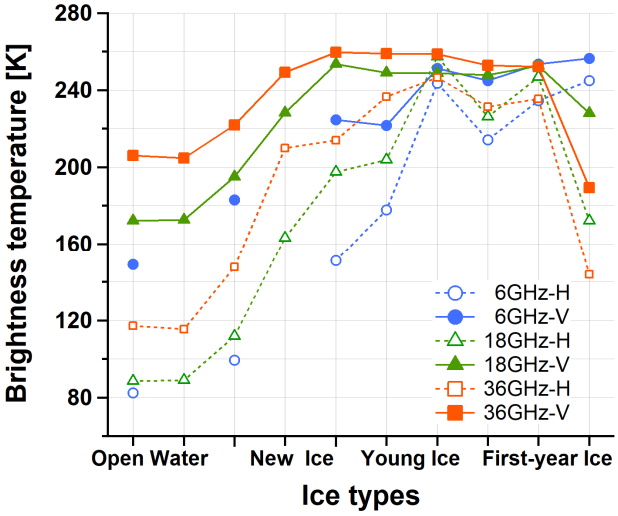

Figure 3 Results of onboard PMR observations. The horizontal axis and the vertical axis mean the sea ice type, and the brightness temperature, respectively.

Dynamic ocean topography in arctic sea by Envisat/RA-2

Keigo Kageyama[1], Kohei Mizobata[1]
[1]*Tokyo University of Marine science and technology, Japan*

Oceanic heat transport, its pathway and controlling mechanism are indispensable to understand future fate of the Arctic Ocean and sea ice variability. Unfortunately, continuous hydrographic observations covering entire ocean through a year is quite hard, so that we need an alternative method to elucidate the ocean circulation. The dynamic ocean topography (DOT) derived from the satellite radar altimeter SIRAL mounted on CryoSat-2 (CS-2) is one of the important parameters (e.g., Mizobata et al. 2016). However, CS-2 measurements started from late 2010, therefore the long-term or decadal variability of the Arctic ocean circulation is difficult to be analyzed. Before 2010, the earth observing satellites IceSat and Envisat had made observations. Although many efforts were made to understand DOT, the observation period for the former is limited to a few winter months, and the latter has been discussed mainly in the mean field. In this study, we analyzed the measurements by altimeter RA-2 mounted on the Envisat from 2002 to 2012, and calculated DOT. In this study, the sea surface height and DOT was determined by two different methods described below. The first method we tried (almost same as in Mizobata et al., 2016) was to estimate DOT in open-water area only where is detected by using the parameter Pulse Peakines (removing point data of peakiness which become indicator of sea ice exeed a certain value). After DOT was estimated, we constructed three-month mean DOT dataset not affected by sea ice. Based on the first method, monthly DOT could not be created due to few available DOT(resulting three month mean DOT by this method is shown in Figure. 1). The second method, which we call EOF filtering, first relaxes the thresholds PP and builds a monthly average DOT dataset containing the error values. We then apply principal component analysis to define the higher-order modes as errors and reconstruct the DOT dataset with only the lower-order modes of EOF. In this presentation, we compare the DOT datasets by the two methods and discuss the consistency with CS-2 data.

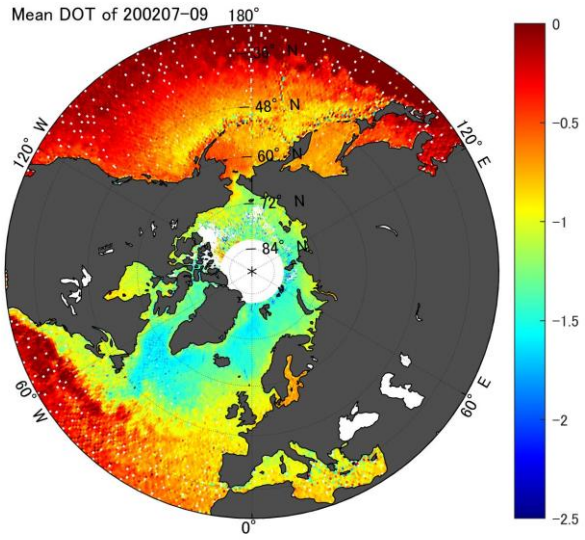

Figure. 1. Three month mean DOT after removing DOT affected by sea ice by peakiness threhold(Peakiness > 0.028)

References

Mizobata,K. et al. (2016) : Wintertime variability of the Beaufort gyre in the Arctic Ocean derived from CryoSat-2/SIRAL observations . JGR-Oceans , 121(3), 1685-1699.

Numerical Weather Predictions to support the Ice Core Drilling Expedition 2021 at SE-Dome, Southeastern Greenland Ice Sheet

Akihiro Hashimoto[1], Teruo Aoki[2], Yamasaki Tetsuhide[3], Sumito Matoba[4], Masashi Niwano[1], Tomonori Tanikawa[1], Koji Fujita[5], and Yoshinori Iizuka[4]

[1]*Meteorological Research Institute, Japan Meteorological Agency*

[2]*Arctic Environment Research Center, National Institute of Polar Research*

[3]*Avangnaq*

[4]*Institute of Low Temperature Science, Hokkaido University*

[5]*Graduate School of Environmental Studies, Nagoya University*

A shallow ice core drilling expedition was conducted from May 9 to June 14, 2021 at the SE-Dome site (67°11′30.14328″N, 36°28′ 12.77075″W, 3160.7 m a.s.l.), southeastern Greenland Ice Sheet (Iizuka et al., 2021), following the last drilling in 2015 at almost same location (Iizuka et al, 2016). During the expedition, we performed numerical weather prediction in the supercomputer at Meteorological Research Institute, and provided local weather forecast everyday for safe operation in the extreme environment of high-altitude ice sheet as carried out in the previous expedition in 2015 (Hashimoto et al., 2017). Expedition crews sent back a weather report every day for evaluation of our numerical weather prediction model. Major severe weather events such as blowing snow, blizzard or snowstorm were reported from May 21 to the early morning on May 27 (E1), from May 28 to 30 (E2), and from June 4 to 6 (E3). Figure 1 shows the time-latitude cross section of weather parameters from the JMA's global analysis data along the longitude 36°W. During the major severe weather events, intense easterly wind hit the SE-Dome site.

The numerical weather prediction was performed twice per day. Each time, simulation was first performed with a horizontal resolution of 5 km (5 km-NHM) in a computational domain of 4000 km × 3500 km which covers the Icelandic islands, Svalbard Islands, and Norwegian Sea as well as Greenland. Next, simulation with a horizontal resolution of 1 km (1 km-NHM) was performed in the subdomain of 650 km × 650 km centered at SE-Dome. Predicted air temperature, wind speed and direction at SE-Dome by 5km-NHM basically well agreed with observation, although predicted air temperature tended to have larger bias when wind speed was week (Fig. 2).

During the event E1 (from May 21 to the early morning on May 27), the SE-Dome site was hit by intense wind associated with low pressure systems passed through the southeast offshore of Greenland. According to the simulation results on May 25, intense easterly wind formed mountain wave over SE-Dome. Surface wind speed and potential temperature on the lee side of SE-Dome was greater than the upwind side, which corresponds to the distribution of vertical wind; updraft and downdraft over the upwind and downwind side of SE-Dome, respectively.

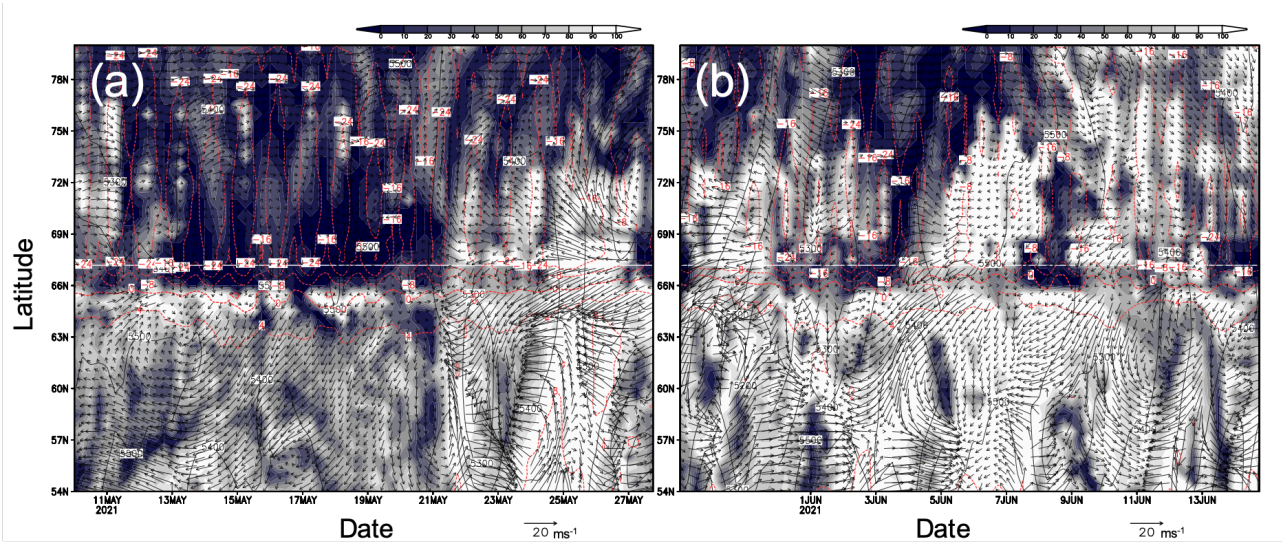

Figure 1. Time-latitude cross section of cloud coverage (shade), surface air temperature (red contour), 500 hPa geopotential height and wind vector along the longitude of 36°W (a) from May 10 to 28, and (b) from May 28 to June 15, 2021. The white line indicates the location of SE-Dome.

Dynamical features of topographically induced air flow around SE-Dome and their effects on cloud/precipitation throughout the drilling expedition will be discussed in the symposium.

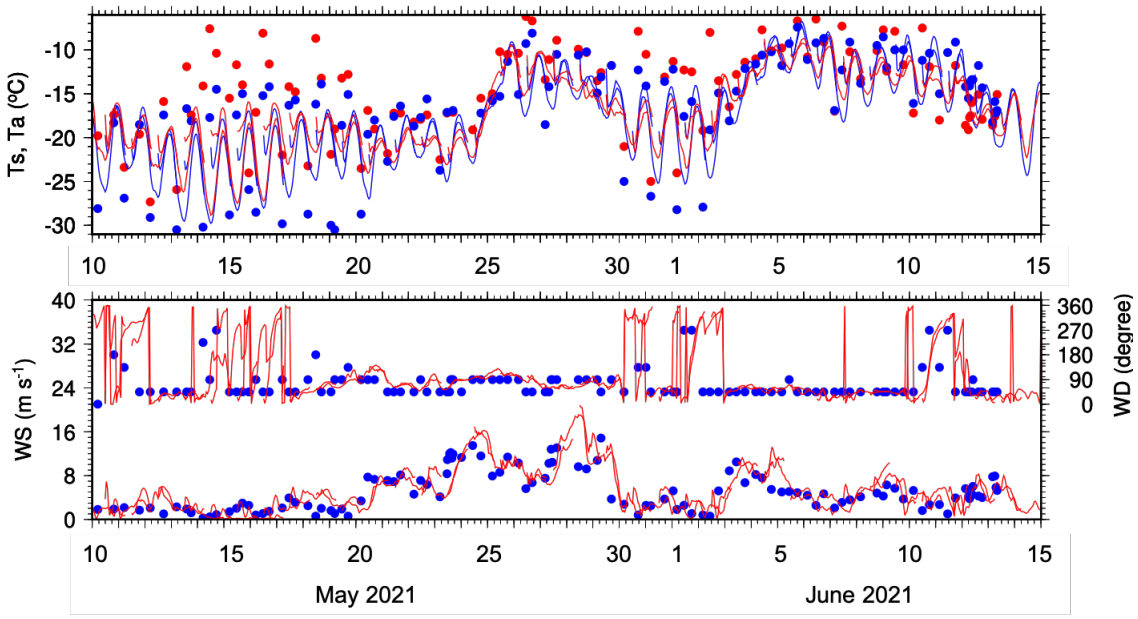

Figure 2. Results from observation (colored dot) and simulation (colored line) with 5km-NHM for (a) Snow temperature (blue) and surface air temperature (red), and (b) wind speed and direction from observation (blue dot) and simulation (red line).

Acknowledgements

This study was supported by MEXT/JSPS KAKENHI Grant Number 18H05292, 21H03582 and the Arctic Challenge for Sustainability (ArCS II) Project, Program Grant Number JPMXD1420318865.

References

Hashimoto, A., M. Niwano, T. Aoki, S. Tsutaki, S. Sugiyama, T. Yamasaki, T. Iizuka and S. Matoba, Numerical weather prediction system based on JMA-NHM for field observation campaigns on the Greenland ice sheet, Low Temp. Sci., 75, 91-104, 2017.

Iizuka, Y., S. Matoba, T. Yamasaki, I. Oyabu, M. Kadota, and T. Aoki, Glaciological and meteorological observations at the SE-Dome site, southeastern Greenland Ice Sheet. Bull. Glaciol. Res., 34, 1-10, 2016.

Iizuka, Y., S. Matoba, M. Minowa, T. Yamasaki, K. Kawakami, A. Kakugo, M. Miyahara, A. Hashimoto, M. Niwano, T. Tanikawa, K. Fujita and T. Aoki, Ice Core Drilling and the Related Observations at SE-Dome site, southeastern Greenland Ice Sheet, Bull. Glaciol. Res., 39, 2021. Accepted.

Is surface darkening occurring over the Greenland Ice Sheet?

Teruo Aoki[1, 2], Rigen Shimada[3], Masahiro Hori[4], Tomonori Tanikawa[5] and Masashi Niwano[5]
[1]*National Institute of Polar Research, Japan*
[2]*SOKENDAI (The Graduate University for Advanced Studies), Japan*
[3]*Earth Observation Research Center, Japan Aerospace Exploration Agency*
[4]*University of Toyama, Japan*
[5]*Meteorological Research Institute, Japan Meteorological Agency*

The surface albedo reduction or so-called “surface darkening” in the summer season over the Greenland Ice Sheet (GrIS) has been reported based on the ground and satellite observations (e. g., Box et al., 2012; Stroeve et al., 2013; Alexander et al., 2014; Tedesco et al., 2016) in the past decade. Certainly, monthly mean albedo over the GrIS calculated from Moderate resolution Imaging Spectroradiometer (MODIS) snow product (Hall et al., 1995) decreased with a statistically significant trend ($p < 0.01$) in linear regression for July (trend: -0.033/decade) and August (trend: -0.022/decade) from 2000 to 2012. However, plotting the albedo for the period from 2000 to 2020, there are no significant trends for any month from April to September. Then we investigated the interannual trend of surface albedo in detail by dividing the GrIS into different elevation zones or different surface types (snow or ice). No significant trend of the albedo variation from 2000 to 2020 is due mainly to the large albedo fluctuations since 2013. When we plot the interannual albedo variations in different zones at every 1 km elevation including snow and ice surfaces, there are no significant albedo trends in linear regression from 2000 to 2020 in any elevation region. The slope of linear regression in albedo variation is negative in July and August but positive in September, suggesting possible increase of snowfall in September. The difference in the averaged albedo between the first half (2000-2009) and the second half period (2010-2020) (second – first), we refer to “decadal albedo change” hereafter, is negative from June to August and positive in September. The minimum value is -0.023 in July and the maximum +0.011 in September both for the elevation zone lower than 1 km. These tendencies are basically the same for snow-covered areas (excluding bare ice surface). On the other hand, albedo averaged over bare ice areas varied with a statistically significant decreasing trend ($p < 0.01$, trend: -0.018/decade) from 2000 to 2020 for only the lowest elevation zone (< 1 km) in July and the decadal albedo change is -0.018 as well. This could be attributed to an expansion of dark ice extent. From these results, the albedo reduction or surface darkening from 2000 to 2020 was not a statistically significant phenomenon over the entire GrIS or each elevation zone except for bare ice areas at lower elevation in July. However, both the slope of linear regression in albedo variation as well as the decadal albedo change indicate the decrease in albedo for almost areas in summer season. Therefore, we can use the term "surface darkening" over the GrIS but need to take care statistically.

References

Alexander P.M., M. Tedesco, X. Fettweis, R.S.W. van de Wal, C.J.P.P. Smeets and M.R. van den Broeke, Assessing spatio-temporal variability and trends in modelled and measured Greenland Ice Sheet albedo (2000–2013), The Cryosphere, 8, 2293-2312, 2014, doi:10.5194/tc-8-2293-2014.

Box, J. E., X. Fettweis, J. C. Stroeve, M. Tedesco, D.K. Hall, and K. Steffen, Greenland ice sheet albedo feedback: thermodynamics and atmospheric drivers, The Cryosphere, 6, 821-839, 2012, doi:10.5194/tc-6-821-2012.

Hall, D.K., G.A. Riggs and V.V. Salomonson, Development of methods for mapping global snow cover using moderate resolution imaging spectroradiometer data, Remote Sensing of Environment 54, 127-140, 1995, doi:10.1016/0034-4257(95)00137-P.

Tedesco, M., S. Doherty, X. Fettweis, P. Alexander, J. Jeyaratnam and J. Stroeve, The darkening of the Greenland ice sheet: trends, drivers, and projections (1981–2100), The Cryosphere, 10, 477-496, doi:10.5194/tc-10-477-2016, 2016.

Stroeve, J., J. E. Box, Z. Wang, C. Schaaf, and A. Barrett, Re-evaluation of MODIS MCD43 Greenland albedo accuracy and trends, Remote Sens. Environ. 138, 199-214, 2013, doi:10.1016/j.rse.2013.07.023.

Integration test of polar regional climate model and radiative transfer model for development of microwave remote sensing simulator

Rigen Shimada[1,2] and Masashi Niwano[2]
[1]*Japan Aerospace Exploration Agency*
[2]*Meteorological Research Institute*

Since the 1970s, satellite-borne passive microwave radiometers have been observing the global water cycle through monitoring relevant climate variables. The GCOM-W/AMSR2 is currently performing global water cycle observations, providing various geophysical products such as sea ice concentration, atmospheric water vapor content, soil moisture, and sea surface temperature. The Ministry of the Environment of Japan and JAXA are jointly developing GOSAT-GW as a next-generation water cycle observation satellite, and GOSAT-GW will carry AMSR3, the successor to AMSR2, which is expected to inherit the observations made by AMSR2 and advance new science. The AMSR2 and other microwave satellites have been used to observe polar regions, including sea ice concentration and snow depth. In addition, microwave observations are often used to detect large-scale surface melt of the Greenland Ice Sheet, and thus microwave ice sheet observations play an important role in monitoring the rapidly changing physical conditions of the ice sheet. However, the current AMSR2 products developed by JAXA do not include information related to the ice sheet. Therefore, it is necessary to develop a satellite simulator that simulates microwave radiations in order to evaluate ice sheet changes detected by microwave satellite observations and to investigate effects of climate change. Here, we simulate microwave satellite observations by coupling the polar climate model NHM-SMAP (Niwano *et al.*, 2018) with the snow and ice surface radiative transfer model MEMLS (Mätzler and Wiesmann, 1999).

As an initial test, the brightness temperature of the ice sheet surface was calculated by using the snow temperature, volume water content of snow, density, and layer thickness of the snow at the surface simulated by NHM-SMAP as inputs to MEMLS, and was compared with actual satellite observations. The brightness temperature calculated by MEMLS is for the horizontal and vertical polarization of 18.7 GHz. The target date was July 1, 2019, and the daily average values were compared with each other. Atmospheric effects were not considered in this test. As a result, a positive correlation was obtained for the vertical polarization (Fig. (a), r = 0.27), but the correlation was weak for the horizontal polarization (Fig. (b), r = 0.04), indicating a large difference from the actual observation. As the change in brightness temperature due to the volume water content of snow is larger for vertical polarization, the change in brightness temperature of surface snow melt during the summer is captured. On the other hand, the background radiation due to the subsurface layer of snow may not be considered. Therefore, we plan to conduct a test using deeper physical conditions as input values for MEMLS.

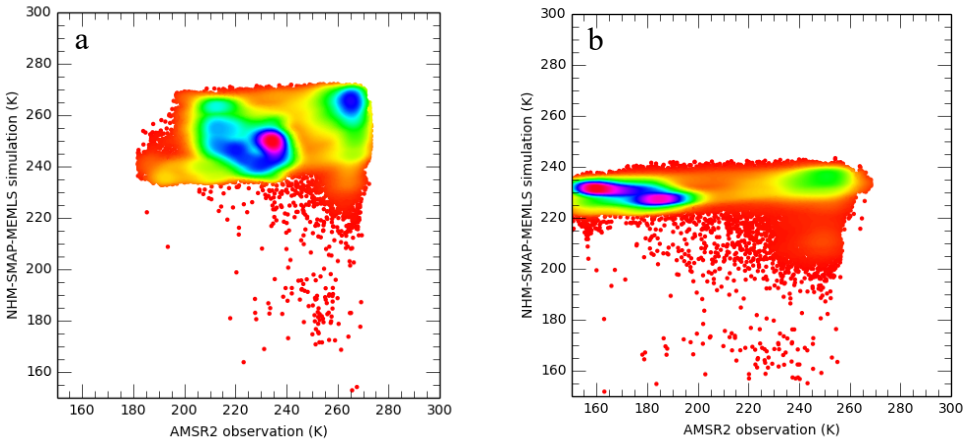

Figure. Comparison of observed and simulated brightness temperature at (a) 18.7 GHz vertical polarization and (b) horizontal polarization.

References

Niwano, M., *et al.*, 2018: NHM–SMAP: spatially and temporally high-resolution nonhydrostatic atmospheric model coupled with detailed snow process model for Greenland Ice Sheet, *The Cryosphere*, 12, 2, 635-655.

Mätzler and Wiesmann, 1999: Extension of the microwave emission model of layered snowpacks to coarse-grained snow, *Remote Sens. Environ.*, 70, 317-325.

Spatial variations in cryoconite holes and phototrophs across an outlet glacier in southwest Greenland

Nozomu Takeuchi[1], Koki Ishiwatari[1], Akane Watanabe[1], Takahiro Segawa[2]
[1]*Chiba University*
[2]*Yamanashi University*

Cryoconite holes are cylindrical water-filled holes formed on the ablating ice surface of glaciers and can be found commonly from alpine glaciers to polar ice sheets in the world (Fig .1). A dark-colored sediment called cryoconite is deposited at the bottom of holes and a liquid water column lies above the cryoconite during the ablation season. Due to the dark coloration of the cryoconite, it absorbs more solar radiation than the surrounding bare ice surface. As a result, the ice below the cryoconite melts faster than the surrounding ice, and cylindrical holes are formed. Since cryoconite holes are the places where liquid water is available on the glacier surface during the ablation season, they are inhabited by diverse microbes, including autotrophs such as algae and cyanobacteria, and heterotrophs such as bacteria, rotifers, tardigrada, and insects. The algae and cyanobacteria usually grow in cryoconite at the hole bottom, and photosynthetically produce organic matter, which sustain the heterotrophs living in the holes. They are finally decomposed again to inorganics by heterotrophic bacteria. Thus, these microbes in different trophic levels form a food web and circulate carbon and nutrients biogeochemically within the holes. The cyanobacteria are mostly filamentous and are often entangled with minerals and other organic particles to form small spherical granules (cryoconite granules), which are the major constituents of cryoconite. As cryoconite holes provide stable habitats for these organisms, the dynamics of cryoconite holes are important to understand microbial ecology on glaciers. Furthermore, the hydrology of cryoconite holes is linked with the porous ice surrounding the holes, called weathering crust, and enables the transport of microbes and nutrients to the other holes, and meltwater streams. Meltwater hydrology on the glacier surface substantially affects the microbial communities. Therefore, understanding the so-called 'biocryomorphology' – the linkages and feedbacks between surface ice structures, cryoconite holes and weathering crust characteristics and microbial communities and cryoconite – is essential to studying supraglacial ecosystems

We investigated spatial variations in cryoconite holes and in characteristics of cryoconite and phototroph communities within the holes along a transect across Issunguata Sermia Glacier in southwest Greenland. There was a distinctive ice surface topography along the transect: flat ice zone in the central part and rough crevasse zone near the margin of the glacier. Cryoconite holes showed distinctive morphology between the two zones: shallower in the crevasse zone and deeper in the flat ice zone. Characteristics of cryoconite were also significantly different between the two zones: more abundant organic contents and higher carbon stable isotope values in the flat ice area. Phototroph communities in the holes consisted of filamentous cyanobacteria and glacier algae and their species compositions were also distinctive between the two zones. Results suggest that presence of crevasses on the ice sheet surface is likely to cause the formation of shallower cryoconite holes, which further affects phototroph communities, and carbon cycles on the ice sheet surface.

Fig. 1 Cryoconite holes on Issunguata Sermia Glacier in southwest Greenland (August, 2017)

River surface temperature and channel width in the Arctic region derived from GCOM-C/SGLI

Masahiro Hori[1]
[1]*University of Toyama*

The Arctic rivers flowing into the Arctic Ocean play important roles in the continental hydrological cycles as well as the ocean-atmosphere energy exchange in the Arctic (Park et al., 2020). Recently, the snow cover extent in the Northern Hemisphere has been shrinking during the past 40 years (Hori et al., 2017). Thus, the temporal pattern of fresh water and heat inflow into the Arctic Ocean through the continental rivers can be considered to change drastically. Nevertheless, the number of the in-situ measurements of river water temperature and discharge is quite small and the availability of those data are very limited. This study aims to derive river surface temperature and channel width of the six Arctic rivers shown in Figure 1 (Ob, Yenisei, Lena, Kolyma, Yukon, and Mackenzie) from remotely sensed images from space using optical sensor SGLI onboard GCOM-C satellite launched in 2017. SGLI has spectral channels in the visible to thermal infrared wavelength regions at the spatial resolution of 250 m, which enables us to monitor river surface temperature and channel width on the continental scale. Analysis of the first two-year SGLI data (2018-2019) reveals that river surface temperature can be retrieved successfully on a near-daily basis within the accuracy of 2.6 K (Hori, 2021). Figure 2 indicates an example of spatio-temporal distribution of river surface temperature along the Lena River channel. SGLI-derived river channel width is also correlated well with in-situ river discharge obtained from Arctic Great Rivers Observatory (Arctic-GRO) datasets, indicating the potential of assessing temporal variations in river discharge from space. In near future, the spatio-temporal changes of the river surface temperature and channel width along the Arctic river channels are planned to be monitored on a near-daily basis using SGLI data. The analyzed river surface temperature and channel widths derived from the first two-year (2018 and 2019) SGLI data are available at the following URL shown below.

River surface temperature and channel width data:
http://www3.u-toyama.ac.jp/rsees/river_data.html

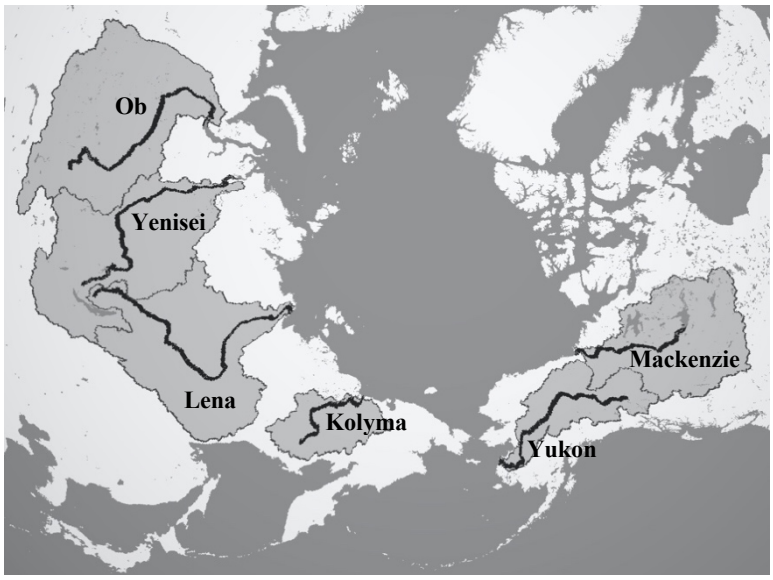

Figure 1. Locations of the six Arctic rivers (thick solid lines) examined in this study.

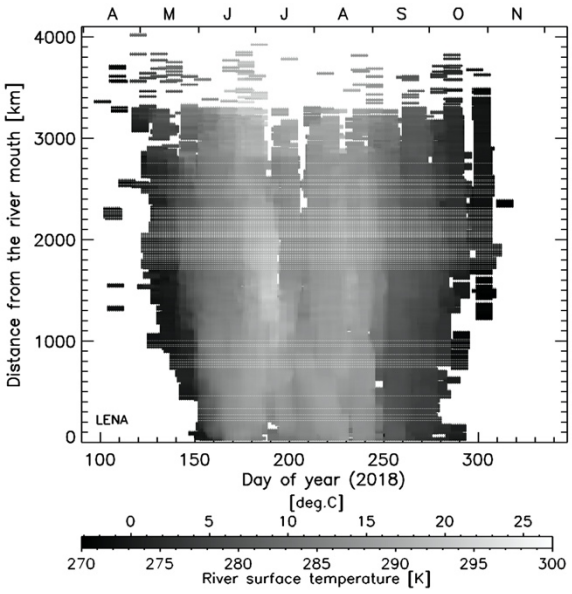

Figure 2 Spatio-temporal distribution of SGLI-derived river surface temperature along the Lena River channel in 2018.

References

Hori, M., Near-daily monitoring of surface temperature and channel width of the six largest Arctic rivers from space using GCOM-C/SGLI. Remote Sens. Environ., 263, 112538. doi: 10.1016/j.rse.2021.112538, 2021.

Hori, M., K. Sugiura, K. Kobayashi, T. Aoki, T. Tanikawa, K. Kuchiki, M. Niwano and H. Enomoto, A 38-year (1978–2015) Northern Hemisphere daily snow cover extent product derived using consistent objective criteria from satellite-borne optical sensors, Remote Sensing of Environment, 191, 402-418, https://doi.org/10.1016/j.rse.2017.01.023, 2017.

Park, H., Watanabe, E., Kim, Y., Polyakov, I., Oshima, K., Zhang, X., Kimball, J.S., Yang, D., 2020. Increasing riverine heat influx triggers Arctic sea ice decline and oceanic and atmospheric warming. Sci. Adv. 6 (45), eabc4699, 2020.

Using deep learning to reveal the distribution of thermokarst

Kosuke Takaya[1], Takeshi Ise[2]
[1]*Graduate School of Agriculture, Kyoto University*
[2]*Field Science Education and Research Center, Kyoto University*

Permafrost in the Arctic is changing rapidly due to climate change. Since much soil organic carbon is stored in the Arctic soil, permafrost degradation affects carbon release. Thermokarst, which is formed by thawing permafrost, is important because it can be used to estimate the degree of permafrost degradation. Remote sensing from satellite images is used to detect and monitor thermokarst. Although satellite images allows us to study a wide area, it requires much effort to detect thermokarst. In recent years, deep learning has been used for environmental monitoring, and it may be able to detect thermokarst quickly. However, few studies have attempted to detect thermokarst by combining satellite images and deep learning. Therefore, in this study, we aimed to detect thermokarst from satellite images of eastern Russia using deep learning. We used Worldview-2 satellite image and created a model using the chopped picture method. This method enables efficient automatic identification of objects by dividing the image into several tens of pixels (Ise et al. 2018). We created a model from the panchromatic and pan-sharpened images using the chopped picture method. Our models were able to detect thermokarst in each image. However, it was difficult to identify the thermokarst from the panchromatic image due to its grayscale. On the other hand, the pan-sharpened image could distinguish the thermokarsts clearly from the surrounding area. This study showed that it is possible to identify thermokarst in a wide area using satellite images at a low cost. Our method may become an effective tool for monitoring the fluctuating environment in the polar regions.

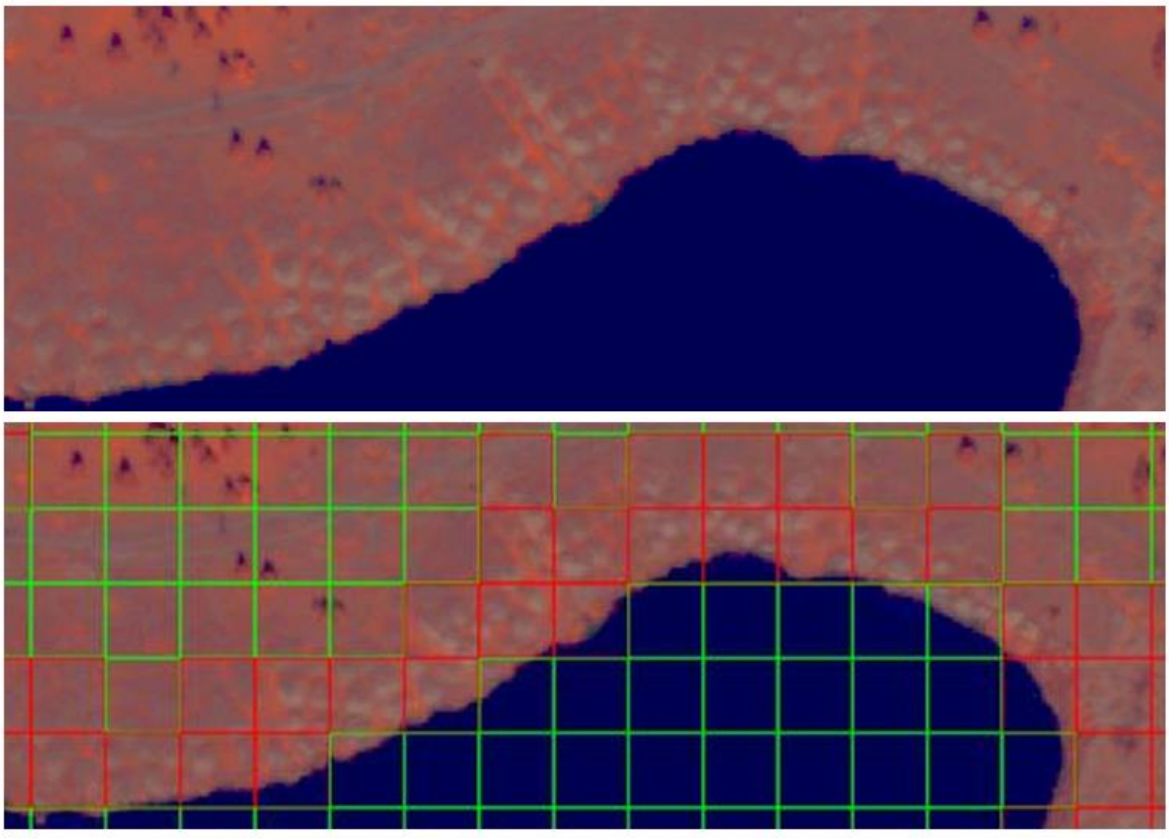

Figure 1. Classification results of thermokarst in Pan-Sharpened Imagery: (a)original images and (b) results. Red squares indicate thermokarst, green indicates others.

References

Ise, T., Minagawa, M., & M. Onishi, Classifying 3 moss species by deep learning, using the “Chopped Picture”methods, Open Journal of Ecology, 8(3), 2018.

Proposal for a new fungus genus isolated from Ellesmere Island, Canadian High Arctic.

Masaharu Tsuji[1], Yukiko Tanabe[2, 3], Warwick F. Vincent[4], Masaki Uchida[2, 3]
[1] *National Institute of Technology, Asahikawa College*
[2] *National Institute of Polar Research*
[3] *The Graduate University for Advanced Studies (SOKENDAI)*
[4] *Université Laval*

Cold environments cover a large part of the Earth, and many ecosystems are continuously exposed to temperatures below 5 °C . Fungi in cold environments can grow and decompose organic compounds even at sub-zero temperatures, and can therefore, play an important role in the biogeochemical cycles of polar ecosystems.

The Walker Glacier (unofficial name) (lat. 83° 00.601'N; long. 72° 12.387'W) is located on the northern coast of Ellesmere Island in the Canadian High Arctic. This region is at the northern limit of Quttinirpaaq National Park, Nunavut, where climate-related effects on the cryosphere have been observed over the last 20 years. GPS measurements on 20 July 2013 from a datum pole that had been installed at this site by Paul T. Walker on 10 July 1959 showed that the glacier had retreated by 71 m, at an average rate of 1.3 m/year over this 54-year period. Repeat GPS measurements at this site during the present study (21 July 2016) showed a further retreat of 10 m, giving an average rate of 3.3 m/year. This 2.5-times faster rate of glacial melting and retreat would indicate a recent acceleration of climate warming at this far northern site.

Subsamples (0.1 g) of the glacial sediment or soil were directly placed on potato dextrose agar (PDA; Difco, Becton Dickinson Japan, Tokyo, Japan) containing 50 μg/mL chloramphenicol and incubated at 10°C for a period of up to 3 weeks.

Fungal samples were chosen for isolation based on colony morphology, and each colony with a different morphology was purified by repeated streaking on fresh PDA. DNA was extracted from fungal colonies, using an ISOPLANT II kit (Wako Pure Chemical Industries, Osaka, Japan) according to the manufacturer's protocols. The extracted DNA was amplified by polymerase chain reaction (PCR), using KOD–plus DNA polymerase (Toyobo, Osaka, Japan). After that, the DNA was purified using Sephacryl S–400HR (Sigma-Aldrich Japan, Tokyo). Sequences were determined using an ABI prism 3130xl Sequencer (Applied Biosystems, Life Technologies Japan, Tokyo).

In total, we isolated 325 fungal strains from the nine glacial sediment samples collected from the Walker glacier site in the High Arctic. Of the 325 fungal strains, 273 strains were succeeded in DNA sequencing. From these 273 strains, two new species of fungi, *Mrakia hoshinonis* and *Vishniacozyma ellesmerensis* are reported (1-2).

Further investigation of the remaining strains revealed that three strains were phylogenetically distinct from the genuses *Glaciozyma* and *Phenoliferia*. Further experiments will be conducted to propose these strains as a new genus, *Ellesmeriozyma*.

References

1. Tsuji M, Tanabe Y, Vincent WF, Uchida M, *Mrakia hoshinonis* sp. nov., a novel psychrophilic yeast isolated from a retreating glacier on Ellesmere Island in the Canadian High Arctic, International Journal of Systematic and Evolutionary Microbiology, 69(4), 944-948, 2019.
2. Tsuji M, Tanabe Y, Vincent WF, Uchida M "*Vishniacozyma ellesmerensis* sp. nov., a new psychrophilic yeast isolated from a retreating glacier in the Canadian High Arctic, International Journal of Systematic and Evolutionary Microbiology, 69(3), 696-700, 2019.

Soil bacterial diversity and function in the Canadian Arctic

Shu Kuan Wong[1], Ryo Kaneko[2] and Masaki Uchida[1,3]
[1]*National Institute of Polar Research*
[2]*BioInsight Co. Ltd.*
[3]*The Graduate University for Advanced Studies, SOKENDAI*

Soil microbes are one of the significant components in the Arctic tundra ecosystem. These microbes play an essential role in the tundra biogeochemical cycles, such as carbon and nitrogen cycling. However, there remains a lot of uncertainty on the microbial diversity and function in the Arctic soil. This paper reports the bacterial diversity and functions in the soil collected from the Canadian Arctic.

A total of topsoil samples from three different latitudes were collected from Whapmagoostui-Kuujjuarapik (herein referred to as KW, Sub-Arctic, 55.3°N 77.8°W), Salluit (Low Arctic, 62.1°N 75.4°W), and Pond Inlet (High Arctic, 72.7°N 78.0°W) during the summer. The soil samples were frozen immediately upon collection and shipped in the frozen state to the National Institute of Polar Research for further analysis. DNA was extracted from the soil sample to investigate the soil bacterial composition, diversity and function. The V4 region of the 16SrRNA gene was subjected to MiSeq sequencing to determine the soil bacterial composition and diversity. The resulting raw sequences from MiSeq sequencing were analyzed using QIIME2 (Ver. 2019.10). Briefly, sequences were clustered into amplicon sequence variants (ASVs) using the DADA2 algorithm and the taxonomic classification of ASVs was carried out using SILVA v132 database as a reference. The functions of soil bacteria from five selected DNA samples were investigated by hybridizing the DNA with functional gene probes available on the GeoChip 5.0M microarray.

The highest microbial diversity can be found in soil samples from the sub- (KW) and high Arctic (Pond Inlet) areas, whereas the low Arctic area (Salluit) has the lowest microbial diversity. Principal component analysis (PCoA) showed that the bacterial communities form two distinct clusters - Salluit and KW clusters – whereas samples from Pond Inlet showed no clear separation patterns. The mean relative abundance of members from the class Acidobacteriia, Actinobacteria, Alphaproteobacteria, Ktedonobacteria and Phycisphaerae were highest in Salluit and lowest in KW. On the contrary, members from the class Blastocatellia, Gammaproteobactria, Planctomycetacia, and Verrucomicrobia were more abundant in KW. The number of functional genes detected by GeoChip 5.0M from the DNA of soil samples collected from KW, Salluit, and Pond Inlet were 89,111, 90,811, and 91,610, respectively. A total of 60,056 genes, 57,891 genes, and 54,726 genes were detected from the cDNA of soil samples collected from KW, Salluit, and Pond Inlet, respectively. A higher number of genes were detected from the soil DNA samples compared with the soil cDNA samples. Most of the functional genes detected from the DNA and cDNA samples originated from bacteria, but genes originating from Ascomycota, Basidiomycota, and viruses were also detected. Predominant functional genes detected from the soil samples were primarily related to metal homeostasis, stress response, carbon cycling, antibiotic resistance, and organic contaminant degradation.

The soil microbial community structure and functions from different regions within the Arctic regions showed that the microbial communities/functions might have different responses or adaptations to local conditions as well as future warming temperatures.